doi.org/10.1002/cmdc.202000895

Chemistry Europe
European Chemical Societies Publishing

VIP *Very Important Paper*

Malaria Pigment Crystals: The Achilles' Heel of the Malaria Parasite

Sergey Kapishnikov,*[a] Ernst Hempelmann,[b] Michael Elbaum,[c] Jens Als-Nielsen,[d] and Leslie Leiserowitz*[e]

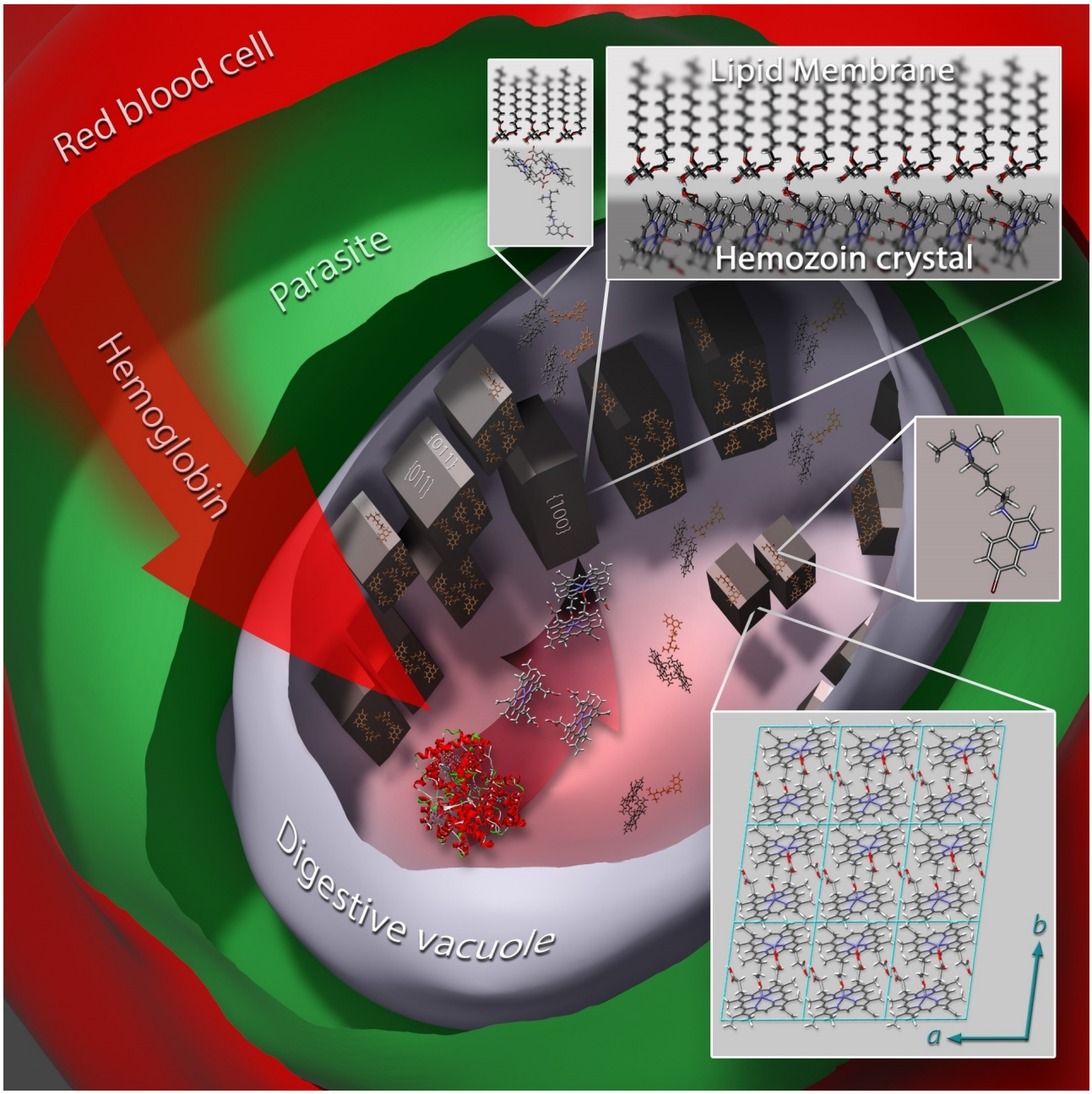

The biogenic formation of hemozoin crystals, a crucial process in heme detoxification by the malaria parasite, is reviewed as an antimalarial drug target. We first focus on the *in-vivo* formation of hemozoin. A model is presented, based on native-contrast 3D imaging obtained by X-ray and electron microscopy, that hemozoin nucleates at the inner membrane leaflet of the parasitic digestive vacuole, and grows in the adjacent aqueous medium. Having observed quantities of hemoglobin and hemozoin in the digestive vacuole, we present a model that heme liberation from hemoglobin and hemozoin formation is an assembly-line process. The crystallization is preceded by reaction between heme monomers yielding hematin dimers involving fewer types of isomers than in synthetic hemozoin; this is indicative of protein-induced dimerization. Models of antimalarial drugs binding onto hemozoin surfaces are reviewed. This is followed by a description of bromoquine, a chloroquine drug analogue, capping a significant fraction of hemozoin surfaces within the digestive vacuole and accumulation of the drug, presumably a bromoquine–hematin complex, at the vacuole's membrane.

1. Introduction

The call for a review of the formation of malaria pigment crystals, namely hemozoin, in the red blood cells infected by *Plasmodium falciparum* is dictated by various considerations, not the least being the need for new antimalarial drugs, in view of developing parasitic resistance to the commonly used ones.[1] Several other factors also contribute to the increasing spread of malaria. Besides climatic and environmental factors, the *Anopheles* mosquito has become increasingly resistant to insecticides and has adapted so as to avoid insecticide-treated surfaces. Human malaria, a tropical, re-emerging infectious disease caused by several types of protozoan parasites of the genus *Plasmodium*, has been a primary concern to humanity for centuries and is now extended to more than 40% of the world's population. It is a disease primarily of the tropics but is also found in many temperate regions of the world including parts of the Middle East and Asia. The disease is responsible for 229 million cases resulting in 409000 deaths in 2019,[2] being particularly fatal among children. Thanks to joint effort of numerous players, including governments and private foundation such as the Bill and Melinda Gates Foundation, this death rate is nearly a half of that 20 years ago. However, due to the current COVID-19 pandemic, 2020 may show a different trend.[3]

Humans are affected by five species of the genus *Plasmodium: falciparum, vivax, ovale, malariae*, and occasionally *knowlesi*. Of these, *falciparum*, the most prevalent species across the globe, is often fatal to humans. The life cycle of the malaria parasite is complex and incompletely understood. During the course of its life cycle, the parasite resides in both the mosquito vector and the human host. The various developmental stages and forms in the latter are depicted and outlined in Figure 1. One of the most extensively studied stages in the human host is that of the red blood cell (RBC), in which the parasite digests hemoglobin in order to grow and multiply. The parasite can digest up to 75% of the RBC's hemoglobin content in a process whereby it is enzymatically cleaved into small peptides, producing free heme (Fe^{II}- protoporphyrin IX (Figure 1) as a by-product, which is toxic to the parasite due to the reactivity of the iron. Thus, the parasite has developed mechanisms to detoxify it. The released heme dimerizes while undergoing a one electron oxidation to produce Fe^{III}-protoporphyrin. The dimers are then sequestered into physiologically insoluble submicron-sized crystals of hemozoin in the parasitic digestive vacuole (Figure 1).

The hemozoin is harmless to the parasite. This process of hemozoin crystallization is now considered as a type of biocrystallization,[4] although from the viewpoint of the human host, pathological crystallization is a more appropriate term.

As alluded to above, a primary cause for the re-emergence of malaria is the development of parasite resistance to antimalarial drugs,[1] in particular some of the commonly used synthetic quinolines. These antimalarials are known to act during the degradation of hemoglobin and subsequent production of malaria pigment crystals in the infected red blood cell. This review will concentrate on the red blood cell stage of parasitic infection, with the focus being on the structure and morphology of biogenic and synthetic hemozoin crystals, the nucleation and growth of hemozoin in a RBC infected by *P. falciparum*, and the mechanism of action of antimalarials such as the quinolines which are believed to inhibit nucleation-growth of hemozoin, as an initial step towards parasitic death.

[a] *Dr. S. Kapishnikov*
Dept. of Chemical Research Support
Weizmann Institute of Science
Rehovot, 7610001 (Israel)
E-mail: skapishnikov@gmail.com
[b] *Prof. E. Hempelmann*
Center of Cellular and Molecular Biology of Diseases
Instituto de Investigaciones Científicas y Servicios de Alta Tecnología (INDICASAT AIP)
City of Knowledge, 0843 (Republic of Panama)
[c] *Prof. M. Elbaum*
Dept. of Chemical and Biological Physics
Weizmann Institute of Science
Rehovot, 7610001 (Israel)
[d] *Prof. J. Als-Nielsen*
Niels Bohr Institute
University of Copenhagen
2100 Copenhagen (Denmark)
[e] *Prof. L. Leiserowitz*
Dept. of Molecular Chemistry and Materials Science
Weizmann Institute of Science
Rehovot, 7610001 (Israel)
E-mail: leslie.leiserowitz@weizmann.ac.il

Supporting information for this article is available on the WWW under https://doi.org/10.1002/cmdc.202000895

2. The Malaria Pigment Crystal: History

The first report of a black pigment in *post mortem* blood and spleen is credited to Meckel.[6] Two years later Virchow attributed pigment formation to malaria.[7] He believed the pigment to be hematin, that is, ferriprotoporphyrin IX hydroxide. This misconception prevailed until 1891 when Carbone made spectroscopic studies and found differences between the malaria pigment hemozoin and hematin.[8] Laveran was able to see the pigmented parasites that cause malaria in 1880,[9] and in 1897 Ross discovered the pigmented cells embedded in mosquitoes, so clarifying its role as a vector of the parasite.[10]

Ninety years later, Fitch and Kanjananggulpan reported conclusively that hemozoin consists of ferriprotoporphyrin IX units.[11] By making use of infrared spectroscopy, X-ray absorption spectroscopy and chemical synthesis, Slater et al.[12] could conclude in 1991 that the heme units are linked between the Fe^{III} ion of one moiety and a propionate oxygen atom of another heme moiety. They hypothesized that the heme units are interlinked to generate a polymer, so yielding an insoluble crystalline product. In 1994, Hempelmann and Marques[13] proposed that the heme units in hemozoin rather dimerize by hydrogen-bonding to form a dimer rather than a polymer since electrophoretic studies yielded only a single band rather than a ladder of separated split products.[13,14] In retrospect, it is also noteworthy that the appearance of well-formed biogenic and synthetic hemozoin crystals displaying slanted end faces with the same angular geometry is a clear indication that the crystals can hardly be composed of polymeric material; the latter, being polydisperse, would have yielded crystals with end faces, not necessarily smooth, but making a right angle with the needle axis. Moreover, given that the synthetic crystals display centrosymmetric $\bar{1}$ morphological symmetry, it was consistent with a centrosymmetric triclinic crystal, which would not be the case for the polymer.

Conventional X-ray diffraction measurements on single crystals of biogenic hemozoin for structure characterization were hardly possible since the crystals were too small in size, but X-ray powder diffraction (XRPD) proved feasible. In a seminal paper, Pagola et al.,[15] applying the powder X-ray diffraction method, reported the crystal structure of synthetic hemozoin, or β-hematin as it is commonly called, to be centrosymmetric, space group $P\bar{1}$, built of Fe^{III}-protoporphyrin

Sergey Kapishnikov is a research scientist with a broad multidisciplinary background. He currently works at the Weizmann Institute of Science having completed postdoctoral terms at the University of Copenhagen and the Helmholtz-Zentrum Berlin, where he studied heme detoxification and the mode of action of antimalarial drugs in Plasmodium parasites. His research interests lie in biogenic crystals as drug targets and in adapting X-ray structural and chemical 3D imaging combined with AI-driven data analysis for biomedical research.

Ernst Hempelmann is a Professor Emeritus at the Center of Cellular and Molecular Biology of Diseases, Instituto de Investigaciones Científicas y Servicios de Alta Tecnología (Republic of Panama), with broad expertise in biochemistry, immunology, medicine and parasitology. He made significant contributions towards understanding and eradication of malaria through research into the detection of P. falciparum glucose-6 phosphate dehydrogenase and nonsequential hemoglobin degradation in malaria parasites, the development of rapid diagnostic tests for malaria, the development of mechanism of silver stain, and the detection of malaria pigment biocrystallization.

Michael Elbaum is a Professor at the Weizmann Institute of Science. He is interested in understanding materials in the living context, crossing the traditional disciplines of biology, chemistry, and physics. His work involves the constant development of microscopy and tomography tools with an ongoing emphasis on Plasmodium.

Jens Als-Nielsen is a Professor Emeritus at the Niels Bohr Institute in Copenhagen. He is known for experimental studies of critical phenomena associated with phase transitions, initially using neutron scattering and later also synchrotron X-ray scattering. He is a co-author of Modern X-ray Physics (Wiley, 2010).

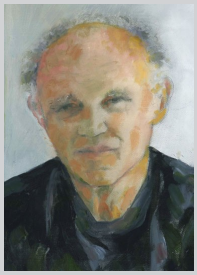

Leslie Leiserowitz cut his scientific teeth in the field of crystal engineering. He joined forces with Meir Lahav in the 1970s to introduce a concept of molecular recognition at interfaces, and so address questions in crystal nucleation, morphology, polymorphism, symmetry and chirality, and crystallization of substances through 2D amphiphilic clusters at the air–water interface. For the latter, they collaborated with J.A.-N., applying grazing incidence X-ray diffraction for structural elucidation of crystalline films at liquid surfaces. Following "retirement" in 2003, Leiserowitz began a study on the nucleation of cholesterol with reference to atherosclerosis, and the mode of action of antimalarial drugs involving the malaria pigment.

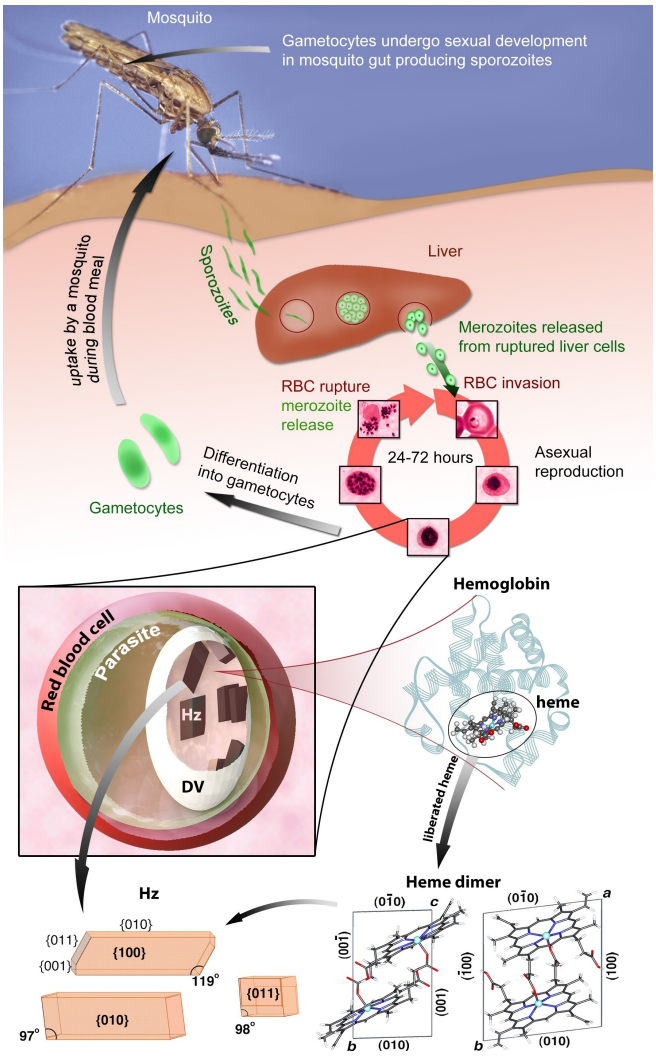

Figure 1. Life cycle of the malaria parasite in humans. The parasite, in the form of sporozoites, is transmitted to humans during a blood meal by the *Anopheles* mosquito. Within an hour, they enter the liver, where they develop and replicate. After 5–15 days, parasites, in the form of merozoites, generated from this phase, are released into the blood stream, where they invade RBCs. Each such parasite consumes about 75% of the cell's hemoglobin content in the digestive vacuole (DV) of the parasite. The heme molecules, released from the process as a by-product, crystallize in the digestive vacuole as hematin dimers into a solid called hemozoin (Hz), the structure and morphology of which are shown. The cell-invading parasite matures during the RBC cycle, eventually rupturing the blood cell to release the "daughter" parasites, which are then free to infect other red blood cells. It is during each such stage that severe conditions of malaria occur. The time spent within a RBC depends on the species. *P. falciparum*, *P. ovale*, and *P. vivax* spend 48 h, whereas *P. malariae* spends 72 h and *P. knowlesi* takes only 24 h to release next-generation parasites. Some of the released "daughter" parasites differentiate into male and female forms, gametocytes, which are sucked up by a mosquito during its blood meal. (Infected RBC images shown in the asexual reproduction cycle are adapted from ref. [5].)

IX molecules reciprocally linked via Fe–O(propionate) coordination bonds into cyclic dimers (Figure 1). These dimers are interconnected via (propionic acid) O–H···O=C hydrogen-bonds forming chains. In addition, a refinement of powder X-ray diffraction data sets of biogenic hemozoin produced by *Schistosoma mansoni* and *Rhodnius prolixus* yielded the same unit cell and structure as synthetic hemozoin.[16] Moreover, hemozoin extracted from red blood cells infected by *P. falciparum* was reported to be "a crystal structure very similar, within the 2.4 Å resolution limit, to that reported for β-hematin".[17] However, there was reason to believe that the hematin dimer in synthetic hemozoin is disordered, comprising four stereoisomers acting as potential crystalline self-poisoners, whereas in biogenic hemozoin the disorder is less pronounced, resulting in crystals of square cross-section, as opposed to the laths typical of the synthetic form. Here we note that the *in-vivo* heme dimerization is believed to be catalyzed.[18] These points shall be elaborated upon at a later stage.

The determination of the crystal structure of synthetic hemozoin by Pagola et al.[15] led them to propose that antimalarial quinoline drugs act by binding to hemozoin crystal faces, following a previous suggestion[19] of a heme polymer-quinoline π–π complexation when it was still believed that hemozoin was a polymer. Such binding would retard or inhibit hemozoin nucleation/growth process, and result in a build-up of the toxic heme and consequently to death of the parasite. Thus, in order to understand the mechanism of action of the antimalarial quinoline drugs, it was necessary to characterize the crystal habit and form (namely overall shape and {*h,k,l*} faces, respectively) of hemozoin and so derive a knowledge of its crystal surface structure.

3. The Link between Crystal Structure and the Morphology of Hemozoin

The morphology of synthetic and biogenic hemozoin has been characterized in terms of its crystal structure, making use of different approaches. A figure of the surface structures of different low-index faces of synthetic hemozoin presented in the Supporting Information (Figure S1) reveals that only the {100}, {010}, {011} faces are relatively flat. All other faces are highly corrugated and so unlikely to form. This simple approach[20] was complemented by computation of the solvent-free theoretical growth morphology of hemozoin,[21] which yielded a needle-like habit extending along the *c*-axis, exhibiting dominant {100} and {010} side faces, a less-developed {011} and a minor {001} facet (Figure 1). This theoretical morphology corresponding to a particular centrosymmetric isomeric hematin dimer of synthetic hemozoin appears to be very similar in both habit and form to that of the biogenic hemozoin crystals with distinct faces from various parasites, in particular *P. falciparum*.[21,22] This match suggests that the effect of the liquid medium on the different faces of hemozoin must be similar. The assigned {*hkl*} indices of the crystal faces of synthetic hemozoin were experimentally established by transmission electron microscopy images coupled with electron diffraction patterns.[23]

4. The Nucleation of Hemozoin Crystals

As already mentioned above, the primary mechanism of heme detoxification is its crystallization into inert hemozoin in the parasite's digestive vacuole. However, there is still considerable debate about how these biogenic crystals form.

Several mechanisms of hemozoin crystallization within the digestive vacuole are discussed in the literature: promotion by histidine-rich proteins in the aqueous environment,[24] growth within neutral lipid bodies,[25] or that certain lipids promote hemozoin formation.[26] The first mechanism has been contested on the basis of two different studies.[25b] The report that the crystallization of the heme is promoted by containing it to a lipid environment, arises from low solubility of heme in water, given the aqueous medium of the digestive vacuole. An electron microscopy study of ultrathin sections of the digestive vacuole stained with malachite green revealed hemozoin crystals enveloped by what was claimed to be neutral lipid droplets and thus apparently formed therein.[25a] These authors have also identified mono-acyl- and di-acyl-glycerol lipids in close association with the sucrose-purified hemozoin using mass spectroscopy. Fitch et al. claimed that certain unsaturated lipids unequivocally promote hemozoin formation.[26] Egan and co-workers reported fast synthetic hemozoin formation near octanol/water, pentanol/water and lipid-solution/water interfaces.[29] However, the lipid as monolayer at the water surface was not observed via grazing incidence X-ray diffraction,[30] which is consistent with their later finding of synthetic hemozoin nucleated at the surface of lipid particles.[31]

Our hypothesis had been that hemozoin nucleates at the membrane–aqueous interface of the digestive vacuole, a concept based on templated nucleation of molecular crystals via amphiphilic crystalline monolayers at the air–aqueous solution interface[32] and of oriented crystallization of synthetic hemozoin as studied at a solid-solution interface.[30,33] To the parasite there is also the advantage of heterogeneous crystalline nucleation at a lipid membrane–liquid interface by crystallizing more rapidly rather than in the liquid lumen of the digestive vacuole. In addition, an early electron microscopy report by Goldberg et al.[34] described a cluster of mutually aligned hemozoin crystals within the digestive vacuole, suggesting nucleation at a common interface.

It is difficult to reconcile the claim of hemozoin crystals embedded within lipid droplets with the concept of induced nucleation of hemozoin at the membrane lipid head group-water interface. A preliminary characterization of hemozoin alignment was made using nanoprobe X-ray diffraction and X-ray Fe-fluorescence on dried infected red blood cells.[35] The data were interpreted in terms of clusters of hemozoin needle-like crystals aligned in parallel with their {100} faces adjoined to a curved surface. To ascertain the hemozoin crystal orientation and whether the crystals are indeed enveloped in lipid droplets, we made use of real-space electron and X-ray microscopy tools. Cryogenic soft X-ray tomography (cryo-SXT, Figure 2a) is uniquely suited to examine the above questions because image contrast can be interpreted quantitatively. X-ray illumination energies were chosen to lie between the atomic absorption edges of carbon and oxygen, from 280 to 530 eV. In this X-ray energy range, called the "water window", lipids and other dense organic matter are much more highly absorbing than the surrounding aqueous medium as is evident from Figure 2b. Indeed, hemozoin, by virtue of its Fe and high carbon content, is strongly absorbing. The basic principles of X-ray tomography is outlined in Figure S2. Cryo-SXT had already been applied by

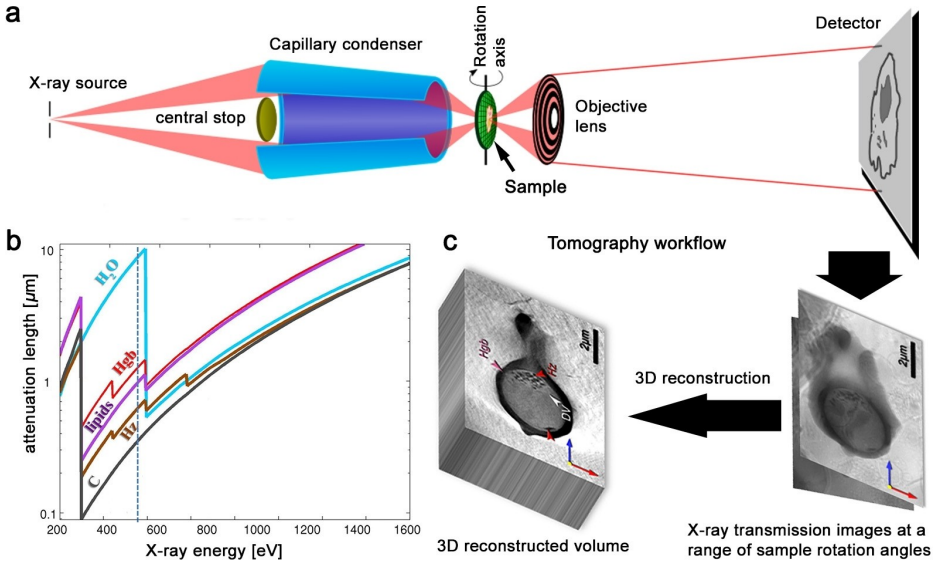

Figure 2. Schematic view of the steps involved in the soft X-ray tomographic procedure. a) The experimental setup, comprising the X-ray source, a central stop, the X-ray condenser, the rotating sample, an objective lens that directs the X-ray to a 2D, as detailed in refs. [27] and [28]. b) The X-ray attenuation lengths of carbon (C), hemozoin (Hz), lipids, hemoglobin (Hgb), and water (H_2O) for X-ray illumination energies ranging from 200 to 1600 eV. Within the so-called "water-window" from 280 to 530 eV, between the atomic absorption transitions of carbon and oxygen, lipid bodies and dense organic matter would appear dark while the aqueous medium would be bright. c) The tomography workflow involving measurement of a series of X-ray transmission images at different rotation angles of the sample to allow generation of the 3D reconstructed volume of the sample.

others to study stage progression and hemoglobin consumption in *Plasmodium*.[36]

The long attenuation length of the soft X-rays in water reaching 10 μm, permits direct observation of intact cells in the vitrified state and avoids the stages of chemical fixation, dehydration, embedding, and sectioning normally required for electron microscopy.

Representative cryo-soft X-ray tomography reconstructions and electron microscopy images of infected red blood cells in trophozoite and schizont stages, taken primarily from our published data,[37] are displayed in Figure 3. The digestive vacuole is clearly visible in the cells, as are numerous hemozoin crystals within. Hemozoin crystals in an early trophozoite stage parasite (Figure 3a) lie side by side all in close proximity to the inner membrane surface of the digestive vacuole, which takes a flattened shape. However, it is not uncommon to observe late stage trophozoites in which a sizeable fraction of hemozoin crystals are found in the lumen of the digestive vacuole, which now assumes a "swollen" shape. In a multinuclear schizont analyzed,[37b] there are several clusters of larger crystals located in the central region of the digestive vacuole, with a number of smaller crystals close to its inner membrane surface.

We had examined in detail the oriented alignment of crystals adjacent to the digestive vacuole membrane,[37b] as exemplified in Figure 3c_3,c_4. This led us to conclude that it is highly unlikely that the crystals would appear oriented unless a common template had been involved in their nucleation.

A quantitative soft X-ray tomographic analysis of the digestive membrane thickness of the trophozoite as well as an image analysis of electron micrographs of particular trophozoites (cf. Figure S3), both yielded a 4–5 nm membrane thickness.[37a] The lipid membrane of the digestive vacuole is thus mainly a bilayer suggesting that the {100} oriented hemozoin crystals are nucleated primarily via the inner of the

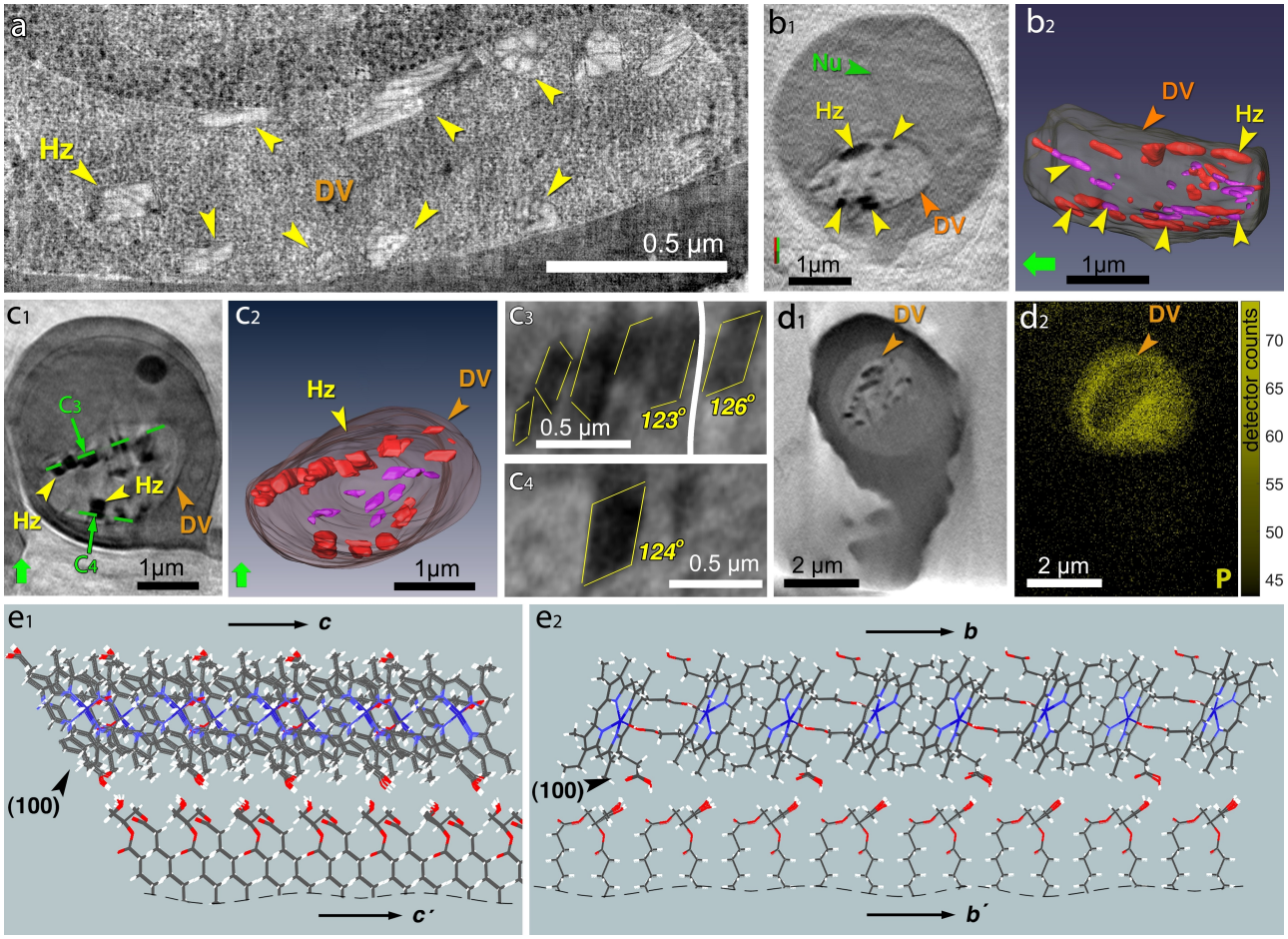

Figure 3. a) A reconstructed tomographic section of the digestive vacuole (DV) of an early-stage trophozoite by electron microscopy, showing hemozoin (Hz) crystals lining the membrane. b_1), c_1) Slices through soft X-ray tomographic reconstructions of two infected red blood cells, each in a trophozoite stage. b_2), c_2) Surface rendering of the digestive vacuole displays hemozoin crystals close to the membrane colored in red, and the remaining crystals in violet. c_3), c_4) Hemozoin crystals from slices through the SXT reconstruction of the digestive vacuole parallel to the membrane marked with green dashes lines in panel (c_1) reveal a common orientation with the crystal *c*-axes lying parallel (c_3). Vertex angles close to 120° indicate that the {100} faces adjoin the digestive vacuole membrane in both (c_3) and (c_4). d_1) The digestive vacuole and hemozoin crystals are apparent in the slice reconstruction of this infected RBC; d_2) the corresponding phosphorus (P) X-ray fluorescence map reveals P atoms distributed across the parasite and distinctly delineated along the membrane of the digestive vacuole, thus indicating that the membrane is composed of phospholipids, and perhaps neutral lipid molecules. e_1), e_2) Model arrangements of the nucleation interface between a diacyl-D-glycerol layer and the (100) face of hemozoin, as viewed along two directions. Reprinted from our previous studies, ref. [37a]. Copyright: 2014, American Chemical Society and ref. [37b]. Copyright: 2012, National Academy of Sciences.

membrane's two leaflets. We have argued that such a leaflet, embodying mono- and di-acyl lipids with appropriate OH or NH bearing head groups, may catalyze hemozoin nucleation by stereospecific and lattice match to the {100} crystal face (Figure 3e), involving a two-dimensional nucleation aggregate of ~100 molecules.[37] In this respect, it is noteworthy that the digestive vacuole membrane displays a phosphorus X-ray fluorescence signal (Figure 3d), implying the presence of phospholipid molecules.

Evidence has been provided, via direct observation by soft X-ray tomography, that hemozoin crystals are not enveloped in lipid droplets during the various stages of trophozoite development.[37] This evidence is further substantiated in Figure 4a, b by reconstructed soft X-ray tomograms of infected red blood cells displaying hemozoin crystals in sharp contrast to the grey scale background. Moreover, a simulation of these hemozoin crystals enclosed within lipid droplets, as shown in Figure 4c, d, complemented by Figure S4, would have been clearly visible.

We conclude that hemozoin is by and large nucleated at the inner membrane surface of the digestive vacuole. As the parasite matures, hemozoin generally detaches itself from the nucleating membrane and continues growing in the lumen of the digestive vacuole. However, questions related to the pathway and rate of hematin dimer navigation as a soluble species in an aqueous medium en route to crystallization still have to be addressed.

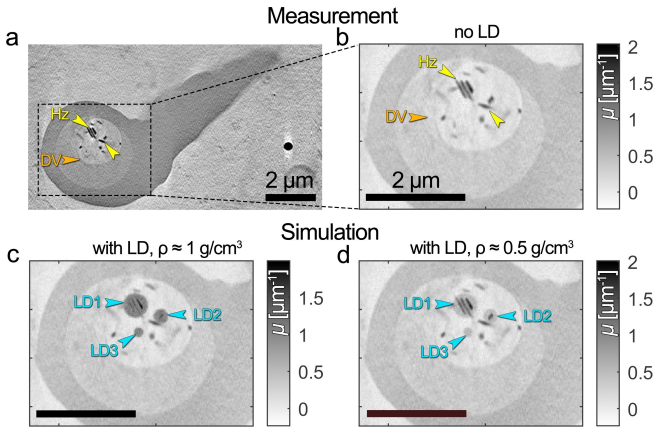

Figure 4. Simulation of lipid droplets of different densities in a soft X-ray tomographic slice through a *Plasmodium*-infected red blood cell featuring the DV containing hemozoin crystals (Hz), a selection of which is marked by yellow arrows. a) Virtual slice through an experimentally derived 3D tomographic reconstruction of a *Plasmodium*-infected RBC. b) Magnification of the *Plasmodium* parasite in this RBC. The grayscale values are now rescaled to match the linear absorption coefficients of the measured material. c) Simulation of the tomographic image had it contained three lipid droplets LD1, LD2 and LD3 with diameters of 500, 300 and 200 nm, respectively, and with a density of 1 g/cm^3 engulfing hemozoin crystals. d) Simulation of three lipid droplets of the same size and location but with a density of 0.5 g/cm^3.

5. Growth of Biogenic Hemozoin Crystals

The growth of hemozoin in the digestive vacuole of the red blood cell infected by *P. falciparum* was elucidated primarily via synchrotron cryo-soft X-ray tomography and atomic element X-ray fluorescence.

The hemozoin content in the digestive vacuole was determined as a function of parasitic age (Figure 5), which yielded an *in-vivo* rate of crystallization of ~7000±2300 heme monomers/s during the trophozoite stage.[38] At this rate, by the end of its red blood cell cycle, the parasite would consume between 37 and 74% of hemoglobin in the red blood cell. Our analysis had also revealed a considerable amount of undigested hemoglobin in the digestive vacuole in a mid-trophozoite stage parasite, with an estimated concentration of 3.3±2 mM, corresponding to $8.8 \pm 6 \times 10^6$ molecules of hemoglobin in freely diffusible space in the digestive vacuole (Figure 5). The corresponding amount of heme would require 1.4 h to crystallize based on the ~7000 heme units/s crystallization rate.

Strikingly, the *in-vivo* rate of crystallization of ~7000±2300 heme monomers/s is similar to the measured *in vitro* rate of heme dimerization ~10^4 heme monomers/s by the heme detoxification protein (HDP) in the study reported by Jani et al.[18a] Indeed, the catalytic role played by the heme detoxification protein (HDP) as an inducer of heme dimerization has also been elaborated upon by Chugh et al.[39] and by Nakatani et al.[18b] The former report the presence of a ~200-kDa protein complex in the digestive vacuole that is required for hemoglobin degradation and hemozoin formation. This complex contains several parasite proteins, including the heme detoxification protein. To functionally characterize this complex, Chugh et al.[39] developed an *in vitro* assay using two of the proteins (falcipain 2 and the heme detoxification protein) present in the complex to show that they associate with each other to efficiently convert hemoglobin to hemozoin. Nakatani et al.[18b] reported four essential histidine residues involved in the heme dimerization process by the heme detoxification protein. Replacement of any or all of these four his residues by alanine, resulted in a reduction in the hemozoin formation activity to approximately 50% of the wild-type protein. Given also that the heme detoxification protein binds two equivalents of heme per molecule,[40] the formation of the hematin dimer at a catalytic site of the protein has been proposed by Nakatani et al.[18b]

The principle of X-ray fluorescence analysis, as applied to a RBC infected by a malaria parasite, is depicted in Figure S5 and presented in the article "Biochemistry of malaria parasite-infected red blood cells by X-ray microscopy".[41] In order to derive reliable estimates of the amount and concentration of the different atomic elements in the various organelles of the cell, we made use of its three-dimensional shape obtained from cryo-soft X-ray tomography measurements. By such means we have analyzed X-ray fluorescence signals obtained from S and Fe atoms in pristine RBCs yielding an atomic ratio close to 3:1, which matches the 3:1 atomic ratio of S:Fe in hemoglobin in a *Plasmodium*-infected red blood cell (Figure S6). These measurements have also revealed the presence of S in the various

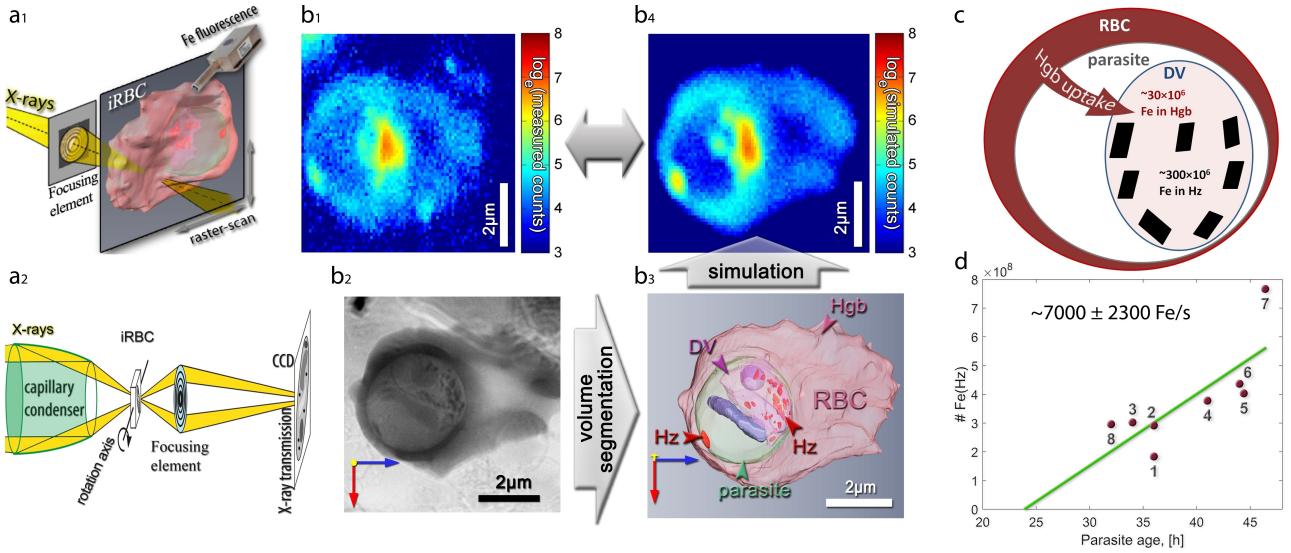

Figure 5. a), b) Infected red blood cell (iRBC) imaged by scanning Fe X-ray fluorescence (top row) and soft X-ray tomography (bottom row), the former is subject to X-ray fluorescence modeling, and the latter to 3D segmentation. a_1) Schematic view of the scanning X-ray fluorescence setup. a_2) Soft X-ray tomography setup. b_1) Fe X-ray fluorescence map of an iRBC. b_2) Corresponding soft X-ray image of the cell. b_3) A 3D volume segmentation of the iRBC derived from a reconstruction of the X-ray tomographic tilt images of the cell. b_4) Simulated 2D Fe fluorescence map derived from the segmentation and an estimate of Fe concentrations in the RBC and the parasitic compartments. The simulated and the measured Fe fluorescence maps become similar when the estimated and actual Fe concentrations closely match. c) The analysis has yielded ~$(30/4)\times10^6$ hemoglobin (Hgb) molecules in the digestive vacuole and ~$(300/2)\times10^6$ hematin dimers in the hemozoin crystals formed. d) Hemozoin Fe content as a function of the parasitic age in eight parasites. The circles are the measured values, and the green line is the fit with equal weights. The slope of the best-fitting line yields the estimated rate of *in vivo* crystallization of ~7000 heme monomers/s. The *x*-intercept is the estimated onset time (~24 h) for hemozoin crystallization.

organelles suggesting that it is possible to determine the relative amount of heme still part of hemoglobin or already released therefrom.

5.1. Assembly-line model for heme detoxification by heme crystallization

Together, the above observations led us to propose an assembly-line model for heme detoxification in the digestive vacuole via hemozoin crystallization,[38] as outlined in Figure 6. This model should yield a reasonable estimate of the average rate at which hematin dimers are supplied to the hemozoin crystals for them to grow to an acceptable size and shape without "crashing out" in the aqueous medium as the heme is so sparingly soluble in water. According to our measurements of hemozoin crystal content as a function of time, *in vivo* heme crystallization occurs at a rate of ~3500 ± 1000 hematin *dimers* per sec, which involves release of the heme monomers from hemoglobin, hematin dimerization, and supply thereof to the hemozoin crystals. Dimerization is catalytically induced by the heme detoxification protein, of which there are 24000 in the digestive vacuole as derived from the article "HDP–A Novel Heme Detoxification Protein from the Malaria Parasite".[18a] We assume, by and large, that the total number of 50 ± 20 hemozoin crystals found in the schizont stage,[37b] with an average size of $130\times130\times450$ nm^3, nucleate and grow simultaneously during the trophozoite stage. Each of the 50 ± 20 crystals is therefore supplied by $(3500\pm1000)/(50\pm20)$ dimers per sec, $\approx70\pm30$ hematin dimers per crystal per sec. On the assumption there is a pronounced tendency for all the heme detoxification protein molecules to simultaneously catalyze formation of the hematin dimers, $24000/(3500\pm1000)$, $\approx7.0\pm2.0$ such protein molecules would generate one hematin dimer each second. In other words, one heme detoxification protein takes 7 sec to dimerize a heme. But buried in this period of time, is the time required for release of the heme from hemoglobin and the time for hematin dimer navigation and occlusion into a growing hemozoin crystal. Therefore, we conclude that a "cluster" of maximally $(70\pm30)\times(7\pm2)\approx(500\pm150)$ heme detoxification proteins would be required to generate 70 ± 30 hematin dimers per crystal per second.

We had proposed a feedback mechanism linking the rate of hemoglobin degradation and heme crystallization, during the assembly-line process (Figure 6).[38] According to our analysis of the results reported by Chugh et al.,[39] the potential rate of hemoglobin degradation by falcipain 2 protease is much higher than the measured rate of hemozoin crystal growth. This analysis suggested that coupling exists between the rate of hemoglobin digestion and the rate of heme dimerization and crystallization. This feedback model is supported by a recent publication on the role played by a lipocalin-like protein, PV5, to control heme crystallization from rodent and human malaria parasites.[42] A knockout of the protein in the human malaria parasite causes what the authors describe as excessive directional branching, indeed what appears to be uncontrolled hemozoin precipitation. Interference with the PV5 expression in the rodent malaria parasite leads to a bootlike shape of the

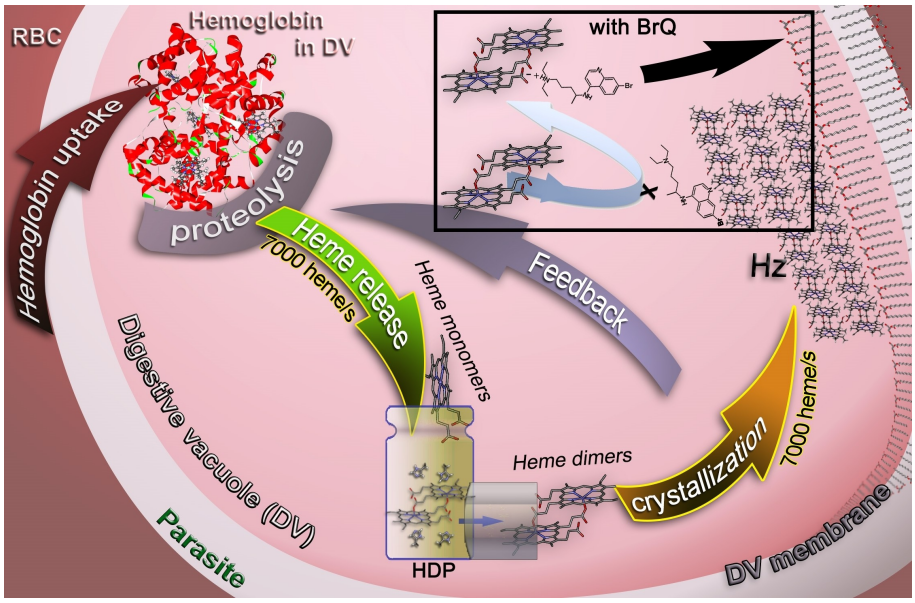

Figure 6. Assembly-line model for hemozoin crystal formation in the digestive vacuole of a RBC infected by *P. falciparum* in the trophozoite stage. Our measurements had shown that *in vivo* heme crystallization occurs at a rate of ~7000 monomers/s (light brown arrow). Note that each hemoglobin molecule contains four heme monomers, so the rate of globin degradation is $^{1}/_{4}$ that of heme monomer release. The measurements also revealed considerable noncrystalline heme in the digestive vacuole and that this heme is mostly contained within hemoglobin shown to be homogeneously distributed (red) in the digestive vacuole, and which had been transported from the RBC cytosol (dark brown arrow). Concomitant with the rate of hemoglobin proteolysis of ~1750 molecules/s, ~7000 heme molecules are released (green arrow). Hematin dimers produced by the heme detoxification protein (HDP) either bind to existing Hz crystals or form new crystals through heterogeneous nucleation at the inner leaflet of the digestive vacuole membrane, in contact with an aqueous environment. Presented in the inset is our overall model for the mode of action of the antimalarial 4-amino quinoline drugs, described in Section 7. Once the drug, exemplified by bromoquine (BrQ), smothers the surface of a Hz crystal, the free hematin dimers, which cannot then be absorbed onto the crystal surface, bind alternatively through an acid–base interaction to the free drugs in the lumen of the digestive vacuole and make their way to the inner-membrane leaflet of the digestive vacuole.

hemozoin crystals, (Figure 7). We interpret this crystal habit in terms of a twin across the "ankle" of the boot about the {011} plane as shown in Figure 7, arising from a partial oversupply of hematin dimers. The surface of the protein PV5 exposes many glutamine ($CH_2CH_2CONH_2$) residues capable of interlinking with the propionic acid groups of the hematin dimers via acid:amide H-bonded pairing,[43] as well as flexible protonated primary amines (NH_3^+), which might form acid-base interactions with the propionic acids, depending upon their state of ionization. The protein PV5 may thus act as a buffer for the supply of hematin dimers to the crystals that grow in an aqueous medium.

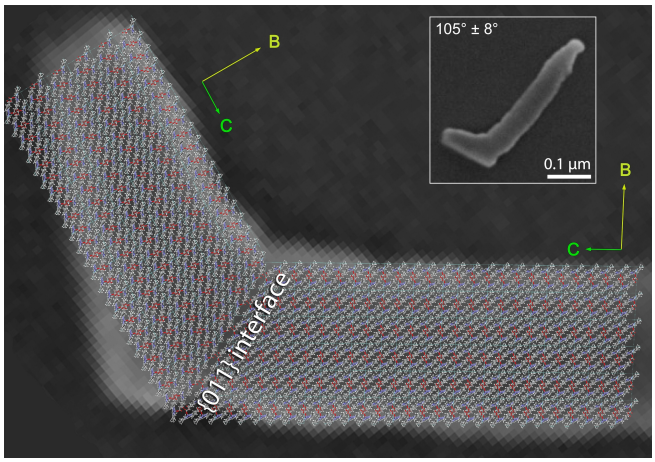

Figure 7. Inset: Boot-like shape of a crystal from rodent malaria parasite as a result of interference with its lipocalin-like protein, PV5 (main figure) The crystal structure of hemozoin, viewed along the *a*-axis, is composed of a 3D array of molecules incorporating the boot-like habit. This habit is simulated by twinning the crystal structure across its {011} plane and is shown superimposed onto the boot. The inset is taken from ref. [42], published under Creative Commons Attribution License 4.0.

6. Towards an Accurate Structure of Biogenic Crystalline Hemozoin

As already alluded to above, the heme dimerization process is catalytically induced by the heme detoxification protein as reported by three different groups.[18,39] This catalytic process would appear to be not only a matter of speed but of proper juxtaposition of the two heme monomers.

Several years ago, the formation of four stereoisomeric dimers of Fe^{III}-protoporphyrin IX in the crystallizing solution of synthetic hemozoin and occlusion thereof into the growing crystals was proposed by Straasø et al.[44] This model was confirmed by Bohle et al.,[45] who found evidence of their occlusion in synthetic hemozoin leading to a disordered

hematin dimer in the crystal. The hypothesis was drawn from the enantiofacial symmetry of the heme molecule (Figure 8a,b), which upon dimerization, would lead to two centrosymmetric ($\bar{1}$) cyclic dimer (*cd*) stereoisomers, and two enantiomeric chiral dimers, *cd*2(+) and *cd*2(−) each exhibiting pseudo-twofold (2) symmetry. We have relabeled the different isomers, to be compatible with the Kahn, Prelog, Ingold convention as proposed by Bohle et al.[45] (Table S1); the two isomers $cd\bar{1}_1$ and $cd\bar{1}_2$, are now named $\bar{1}R/S'$ and $\bar{1}S/R'$ respectively, and the enantiomers *cd*2(+) and *cd*2(−) *2R/R′* and *2S/S′* respectively. The possible vinyl (C–CH=CH_2) sites of the hematin dimer are depicted in Figure 8a, b, and all four dimers are portrayed in Figure 8c. A schematic view of these four isomeric dimers, where the heme molecules are replaced by mittens in order to highlight the differences in structure, is presented in Figure S7. Density functional theory indicates that only minor computed energy differences exist between the four dimers.[46] A subset of these four isomers present in solution could act in a manner akin to a "tailor-made" crystal growth inhibitor,[47] in other words, act as a crystalline self-poisoner of hemozoin, as had been suggested by Buller et al.[21] Indeed, the crystals of synthetic hemozoin are typically thin laths with a dominant {100} side face (Figure S8), which is consistent with the observation that synthetic hemozoin crystals exposing a well-developed {010} side face are not frequently encountered (Figure S8). By comparison, both biogenic hemozoin crystals from *P. falciparum*,[22] and the theoretical growth form of hemozoin,[22] display a square-like cross-sectional shape. This comparison is consistent with the idea that for the crystals of biogenic hemozoin to nucleate and grow as fast as possible, the number of the different (types of) stereoisomeric dimers formed should be *minimal*.

The presence of disordered isomeric hematin dimers in synthetic hemozoin is consistent with the possible presence of a minor phase of synthetic hemozoin, according to nano-crystallography measurements making use of an X-ray free electron laser source.[48] The diffraction data were measured on crystals ranging in size from ~50 to 1000 nm. The authors concluded, on analysis of the data, that there were structural differences between the nano- and macro-sized crystals. We are of the opinion that their nano-sized crystals might correspond to a minor phase of synthetic hemozoin, rather than an early growth stage. A minor crystalline phase is not present in biogenic hemozoin (see below), which would be consistent with a lower amount of isomeric disorder in the biogenic crystal form.

A model of the hematin dimer was adopted by Straasø et al.[44] based on the fact that venous blood in humans retains ~75% of molecular oxygen bound to hemoglobin.[49] It was then assumed that the heme, on release from hemoglobin, retains the O_2 molecule bound to Fe^{II} on the *Re* face of the heme with a computed energy of 24 kcal/mol (see Figure S9 and caption). Hence, the hematin dimer would be primarily formed via the freely accessible *Si* face, leading to isomer *2S/S′* as the dominant structure.

Refinement of a room temperature crystal structure of biogenic hemozoin in terms of isomeric molecular disorder was insufficiently conclusive to point to a crystal structure composed primarily of a chiral dimer. Rather it indicated a mixture of the chiral isomer (*2S/S′* or *2R/R′*) and the centrosymmetric isomer $\bar{1}R/S'$ as shown in Figure S10.[44a]

A more definitive study on the structure of the malaria pigment crystal extracted from *P. falciparum* has recently been undertaken.[50] It involves low temperature (93 K) electron diffraction tomographic measurements of about 30 submicron-sized single crystals, which yielded, on merging over 60000 reflections, 4008 independent and resolved diffraction peaks, comprised of Friedel-related $I(h,k,l)$ and $I(\bar{h},\bar{k},\bar{l})$ pairs. Crystal structure refinement has revealed a mixture of one dominant chiral isomer (*2S/S′* or *2R/R′*) and a minor fraction of the centrosymmetric isomer $\bar{1}R/S'$.

This result indicates that the hematin dimers are formed catalytically via the heme detoxification protein. We presume that the protein operates in tandem with the relatively high concentration of molecular oxygen bound to heme on release from hemoglobin in venous blood. Such hemozoin crystals would be rich in dimers with a *2R/R′* configuration according to the model presented in Figure S9. This would ensure a consistent crystal form in venous blood and in blood that permeates tissues, where oxygenation is considerably lower.

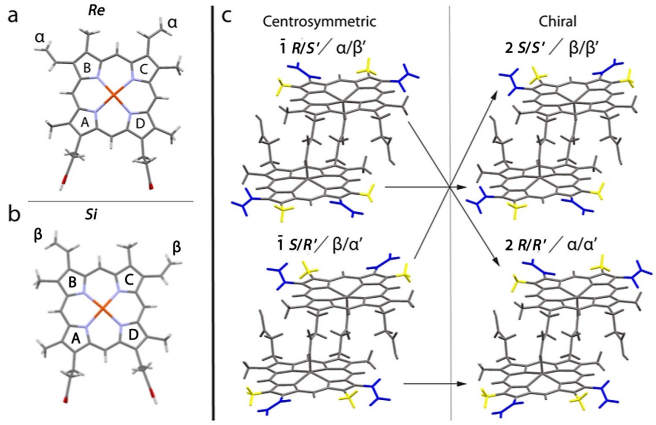

Figure 8. a) Molecular structure of the heme monomer displaying its enantiotopic *Re* face and vinyl (HC=CH_2) substituents at the α sites. b) The corresponding *Si* face and vinyl substituents at the β sites are on the opposite side. The H atoms are excluded. c) The four possible dimeric isomers; two centrosymmetric ($\bar{1}$) structures and two enantiomeric chiral structures in which the hematin monomers are related by pseudo-twofold symmetry (2). The dimer symmetry labels and nomenclature representing the vinyl sites are shown in blue. The lower heme unit is primed to differentiate between the *R/S′* and *S/R′* isomers. The arrows indicate that each chiral dimer is composed of one upper and one lower hematin moiety of the two centrosymmetric dimers (and vice versa).[44] Adapted from ref. [44a] with permission. Copyright: 2014, American Chemical Society.

7. Drug Interference with Hemozoin Formation: The Achilles' Heel of Plasmodium

Armed with knowledge of the crystal morphology of hemozoin, it became possible to address the role played by quinolines and other antimalarials for inhibiting their crystal nucleation and growth, but no less important, how such an effect would be toxic to the parasite.

First, we present an introduction of a general nature on the inhibition of nucleation and growth of molecular crystals via the use of molecular additives. We classify two such types of relevant molecular additives that are crystal nucleation and growth inhibitors; one has a structural complementarity to the surface it binds to, but no structural similarity to the molecules of the host crystal, which we designate as a "capping" molecule; the other class of inhibitors embodies a molecular structure which mimics the host molecule present in the solution, but for a modified moiety, labeled a "tailor-made" additive or inhibitor. It is now well established that minor amounts of such tailor-made additives may dramatically impair the nucleation and growth rate of the host crystal.[47] This effect occurs via selective adsorption of the additive molecule on those surface sites where the modified moiety emerges from the crystal surface, followed by inhibition of regular deposition of oncoming crystal layers.

The adsorption of these two types of auxiliary molecules is schematically depicted in Figure 9. The (001) and (00$\bar{1}$) faces of the crystal (Figure 9a) expose inversion-related "little men" (green vs. yellow) mimicking the hematin cyclic dimer. The tailor-made inhibitor (TMI) is a dimer in which one of the "green" or "yellow" men is wearing a sombrero. This additive can be stereo- and enantio-selectively adsorbed at either a green or yellow site on the (001) or (00$\bar{1}$) faces respectively

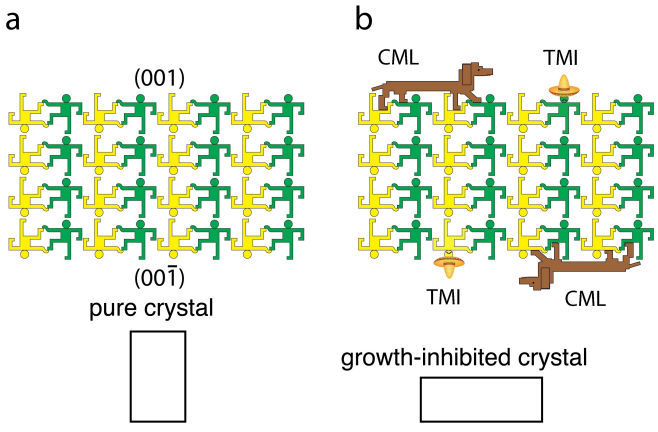

Figure 9. Schematic representation of the hemozoin crystal structure with the heme cyclic dimer depicted by green and yellow "little men". a) The pure crystal structure and morphology. b) The crystal structure and morphology when grown in the presence of a crystal growth inhibitor, which may be of one of two types. Either a tailor-made inhibitor (TMI; a green or yellow man wearing a sombrero) binding to the (001) and (00$\bar{1}$) faces, respectively, or a capping molecule (CML), depicted here as a dachshund, binding stereo-selectively to the {001} faces. Adapted from ref. [20] with permission. Copyright: 2008, American Chemical Society.

(Figure 9b). As for crystal surface adsorption by capping molecules (CML), they can be adsorbed at both yellow and green sites on the (001) and (00$\bar{1}$) faces. This adsorption of the auxiliary molecules will hinder the regular deposition of oncoming molecular layers on the opposite (001) and (00$\bar{1}$) faces, resulting in growth inhibition, as shown in Figure 9b. We shall now examine possible modes of action of antimalarial drugs as capping molecules or tailor-made additives for the inhibition of nucleation/growth of synthetic and biogenic hemozoin.

7.1. The binding of antimalarial quinoline drugs onto hemozoin crystal faces

Quinine (Scheme 1) is found in the bark of the Cinchona tree, indigenous to the Andes Mountains (Figure 10). The bark's use as a treatment for malaria was described in the mid-17th century;[51] the active alkaloid pharmaceutical ingredient, quinine, was isolated from the bark in the early 19th century in a landmark extraction and crystallization undertaking by Pelletier and Caventou.[52] In the 20th century several synthetic quinoline-type drugs such as the 4-aminoquinolines chloroquine and amodiaquine, and the aryl amino alcohol mefloquine (Scheme 1), came onto the market. Of these, chloroquine became the drug of choice, because of excellent clinical efficacy, low toxicity and low cost of manufacture. However, possibly as a result of widespread use, parasitic strains resistant to chloroquine and other synthetic quinolines have evolved.[53] Indeed, it is this resistance, made manifest by reduced drug accumulation in the digestive vacuole,[1,53b,54] that motivated the need for a fuller understanding of the mode of action of quinoline drugs, a knowledge that could be put to use for the design of new antimalarials.

Goldberg and co-workers proposed a mechanism of blockade of hemozoin formation by antimalarial quinolines,[19a] when it was still believed that hemozoin was composed of heme polymers. The idea was that a quinoline molecule caps to an end of a growing polymer via ring-ring van der Waals contacts, thus temporarily retarding its growth. This model was superseded by that of Buller et al.[21] and by Weissbuch and Leiserowitz[20] who, by making use of the theoretical growth form of hemozoin (Figure 1), were able to propose possible binding sites of the antimalarial quinolines on faces of the needle-like hemozoin crystals. In this regard, of crucial importance to the efficacy of quinoline drugs as antimalarials, is the acidic nature of the aqueous medium of the digestive vacuole (pH 4.8 $\pm$0.4). At this pH, chloroquine is protonated both at the tertiary amine and at the quinoline ring N atom.[21] Thus, an additional role of the acidic medium of the digestive vacuole is to enhance the concentration of the weakly basic drug therewithin. The nanomolar concentration of quinoline drugs rises by 3–4 orders of magnitude on reaching the parasitic digestive vacuole, which will be elaborated upon later.

The quinolines (Scheme 1) all protonated at the nonprimary exocyclic amine, can stereo-specifically cap onto the {001} or {011} surface[21] via a (quinoline) amine$\cdots$(heme) propionic acid

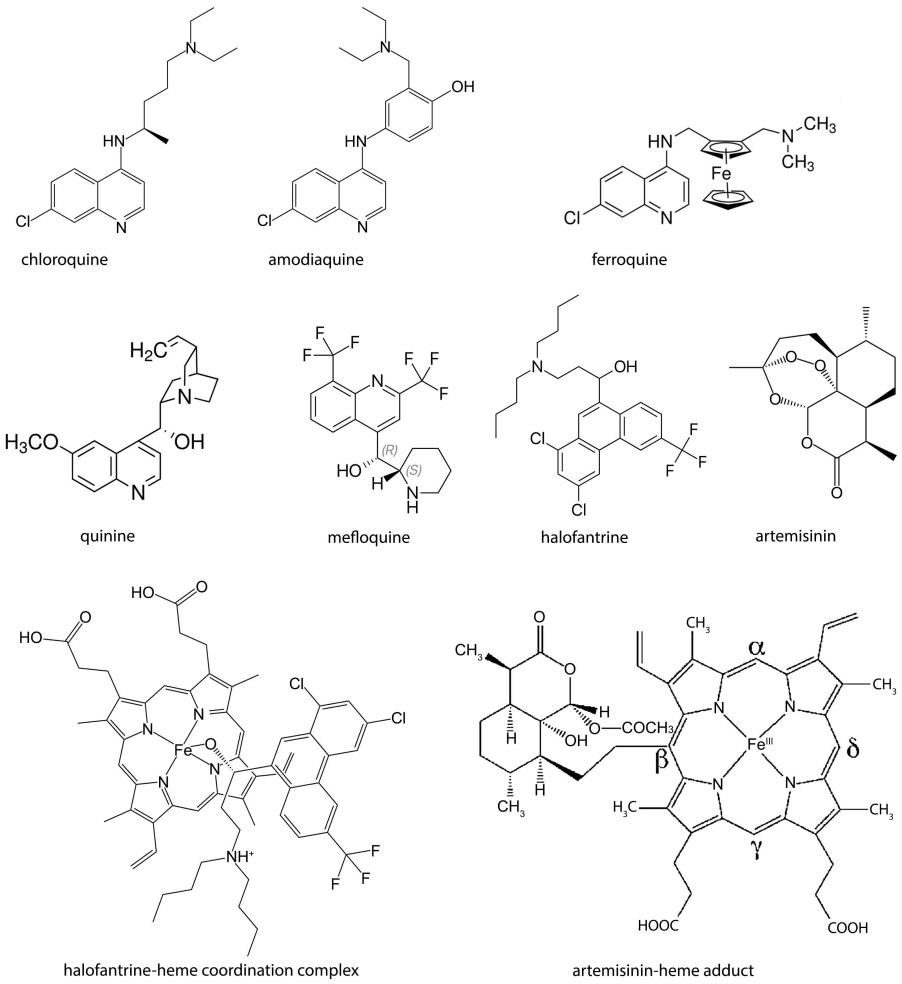

Scheme 1. Several antimalarial drugs of current or past importance that comprise: i) An aromatic quinoline or phenanthrene ring and an exocyclic moiety incorporating an NH group or an OH substituent (such as quinine, mefloquine and halofantrine, possibly capable of coordinating to the heme Fe ion as shown for the halofantrine–hematin complex[55]) and a terminal tertiary amine. ii) Artemisinin, extracted from an ancient Chinese herbal remedy, *Artemisia annua* (sweet wormwood or "qinghao"). The molecular structures of artemisinin and Fe^{II}-heme shown alkylated by artemisinin at the β position[56].

salt bridge and still fit snugly onto the {001} surface, by intercalation of the quinoline rings between the aromatic groups of the hematin dimers (Figure 11a). Far more important is the model for binding to the well-developed {100} side face proposed by Buller et al.[21] and improved upon by Kapishnikov and Leiserowitz in an article by Biot and co-workers.[57] This model involved attractive acid-base ($CO_2^{-}\cdots{}^{+}HN$) interactions between two accessible propionic acid groups of adjacent unit cells on an {100} face and the terminal tertiary amine and quinoline ring of the drug (Figure 11b). This model can be generalized to quinoline drugs, such as chloroquine and other quinolines, with an appropriate distance between its terminal amine and the quinoline ring, so that the drug can attach itself to the two different sites on the hemozoin surface.

By comparison, the aryl amino alcohols mefloquine and quinine (Scheme 1) may, in principle, each form a coordination O–Fe bond with a heme monomer, akin to what was observed in the coordination complex of halofantrine and Fe^{III}-protoporphirin IX (Scheme 1).[55] The mefloquine-heme adduct has been modeled to bind to the {010} face of hemozoin (Figure 11c) as a tailor-made additive.[20]

Finally, we consider inhibition of crystal nucleation/growth of hemozoin as a possible mode of action to account for the widely used antimalarial drug, artemisinin, extracted from an ancient Chinese herbal remedy, *Artemisia annua* (sweet wormwood or "qinghao"). Artemisinin (Scheme 1), is a 1,2,4 trioxane that has been used in China for the treatment of multidrug-resistant *P. falciparum* malaria, but its low solubility in both oil and water has led to a search for more effective and water-soluble derivatives, such as artemether and artesunate.[20] Like the antimalarial drug mefloquine, artemisinin as an in-vivo heme adduct, might act as a tailor-made inhibitor of hemozoin growth.

Heme-artemisinin adducts have been demonstrated in parasite cultures treated with therapeutic concentrations of artemisinin derivatives.[59] Meunier and co-workers characterized the structure of artemisinin-heme adducts (Scheme 1) and identified formation of such adducts in infected mice *in-vivo*.[56,60] Artemisinin forms covalent bonds with heme when incubated

Figure 10. The gathering and drying of cinchona bark in a Peruvian forest. Wood engraving, by C. Leplante, c. 1867, after Faguet. Credit: Wellcome Library Collection no. 20956i.

in a cell-free solution and these same artemisinin–heme adducts appear to form in artemisinin-treated parasites. At micromolar concentrations, artemisinin inhibits hemoglobin digestion by malaria parasites and inhibits hemozoin formation, but this has only been demonstrated in cell-free conditions.[61] Artemisinin can alkylate the heme with equal regioselectivity at various sites to yield different adducts (Scheme 1).[56] It has been postulated that such heme-artemisinin adducts form cyclic dimers with pure heme monomers to yield molecular structures akin to that of a tailor-made inhibitor, which can bind to the different crystal faces of hemozoin (Figure 11d).[20] On the assumption that the mode of antimalarial action of artemisinin follows the above route, we may predict that the synthetic peroxide analogues, whose antimalarial activity has been reviewed by Bray et al.[54] might act similarly.

7.2. Mode of action of antimalarial quinolines in parasitized red blood cells

The question of the mode of the widely used action antimalarial quinoline drugs has been open for centuries. It has been recently narrowed down to how these drugs interfere with the process of crystallization of heme in the malaria parasite. To date, all studies of the drug action on hemozoin crystals have been done either on model systems[23,25c,62] or on dried parasites.[63] The study to be reviewed here was done in actual parasites in their near-native environment, revealing the mode of action of these drugs *in vivo*.

In order to validate the proposed mechanism of action of antimalarial quinoline drugs, we were fortunate to be able to address the following questions as the analysis of the experimental results progressed. What is the concentration of the drug in the digestive vacuole of the parasite? Does the drug indeed bind to the hemozoin crystal faces and persist at these crystal surfaces *in vivo?* If so, would the crystal surface coverage by the drug be sufficient to inhibit regular hematin dimer adsorption onto the crystal faces? Finally, what is the consequence of this inhibition process, for example, can we detect or envisage binding of the drug to uncrystallized hematin dimers in the lumen of the digestive vacuole and what would such a complex do?

With these considerations in mind, we undertook a correlative X-ray microscopy study to establish the mode of action of established drugs like chloroquine via its localization within hydrated malaria parasites in their native, albeit rapidly frozen, environment.[64] We used bromoquine (Figure 12a), a chloroquine analogue, taking advantage of the identifiable X-ray fluorescence signal of the Br atomic substituent, assuming that the drug's molecular biological properties do not differ significantly from those of chloroquine.[64]

We found that bromoquine accumulates in the digestive vacuole, reaching sub-millimolar concentration, exceeding that in the culture medium 1000-fold, confirming previously reported estimates.[65] Of primary importance, 5–15% of hemozoin crystal surface within the parasitic digestive vacuole was covered with the drug (Figure 12b). This coverage should be sufficient to prevent the newly liberated heme in the form of hematin dimers from docking onto the crystal surface, thereby inhibiting hemozoin crystal growth. To provide evidence of strong attachment of bromoquine to the hemozoin crystal surface we compared bromoquine coverage of crystals within

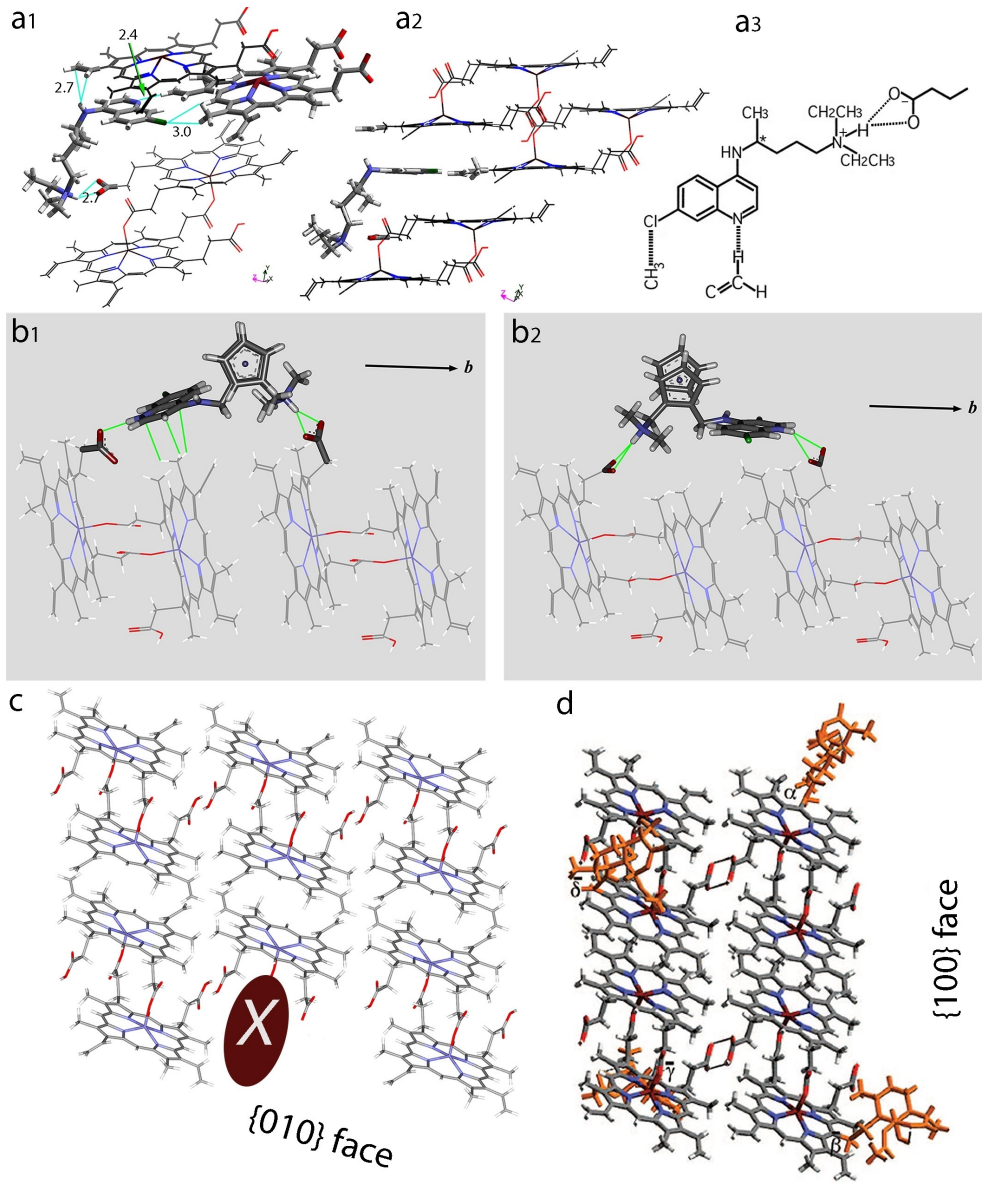

Figure 11. a) Chloroquine bound to the {001} face of a synthetic hemozoin crystal highlighting energetically favorable interactions.[21] a_1) The structure is viewed along a general direction. The {011} face is produced when the highlighted hematin dimer is removed. a_2) The crevice along the *a*-axis within which the drug is intercalated. a_3) Various interactions between chloroquine and the hematin dimer are indicated, including an acid–base interaction, a C–H···N (quinoline) bond,[58] and C–H_3···Cl contacts.[58] b) Two ways of binding of ferroquine (Scheme 1) to the large {100} face of hemozoin, which involves an acid–base interaction between two exposed carboxyl groups of neighboring unit cells, the protonated tertiary amine on one side of the drug, and the protonated quinoline ring on its opposite side.[57] We note that ferroquine can easily be replaced by, say, chloroquine. c) Intermolecular contacts between a quinoline drug with an OH substituent (X, such as in quinine or mefloquine) coordinated to the Fe ion of hematin at the {010} crystal surface viewed edge-on to the plane of the face. d) General view of different artemisinin–hematin dimer adducts, in which the artemisinin moiety is covalently bound to peripheral sites on the hematin dimer, adsorbed on the {100} and {010} crystal faces of hemozoin.[20] Panels $a_{1,2}$, b, and d are adapted with permission from refs. [21], [57] and [20]. Copyright: 2002, 2011, and 2008, American Chemical Society.

the digestive vacuole with those isolated from the parasites (Figure 12c). We found a similar coverage in both cases, suggesting strong interaction between bromoquine and the hemozoin crystal surface.[66]

7.3. The in vivo effect of smothering the crystal faces of hemozoin by bromoquine

Examination of the digestive vacuole in bromoquine-treated parasites also revealed an increased Br signal at its membrane (Figure 13).[66] According to the simulated Br X-ray fluorescence map, which matches the measured map, there is a bromoquine coverage of 5×10^3 molecules per square micrometer of the membrane. Similar but only qualitative observations were made

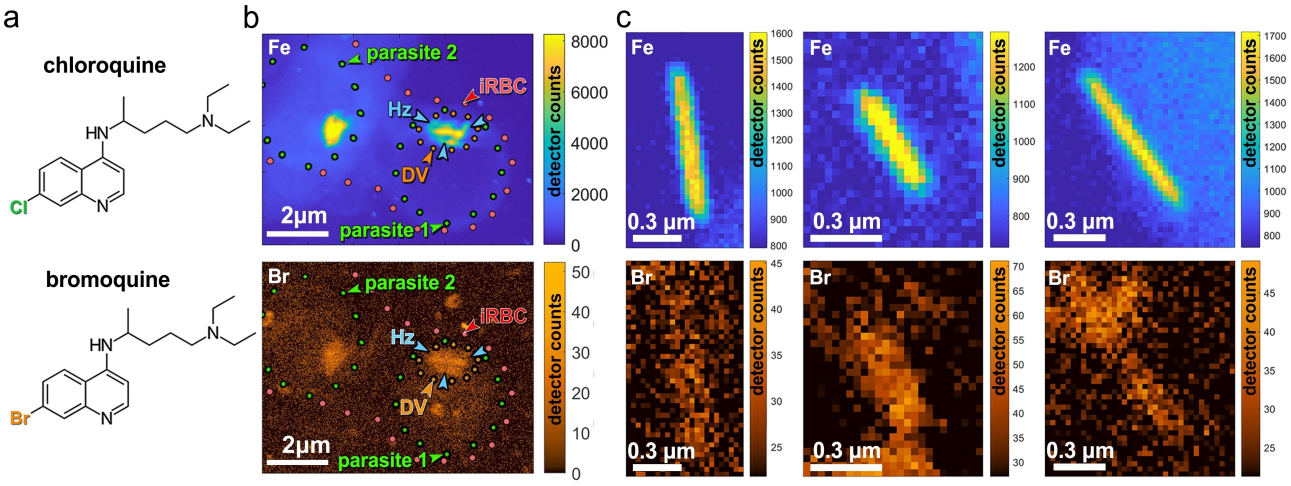

Figure 12. a) Molecular structures of chloro- and bromoquine antimalarial drugs. b) X-ray fluorescence maps of Fe (top) and Br (bottom) in a RBC infected by two parasites. The borders of parasite *1* and its digestive vacuole, shown by dotted lines, have been delineated by cryo-X-ray tomography. c) Fe and Br X-ray fluorescence maps of three isolated, free-floating hemozoin crystals that had been expelled from a ruptured cell.

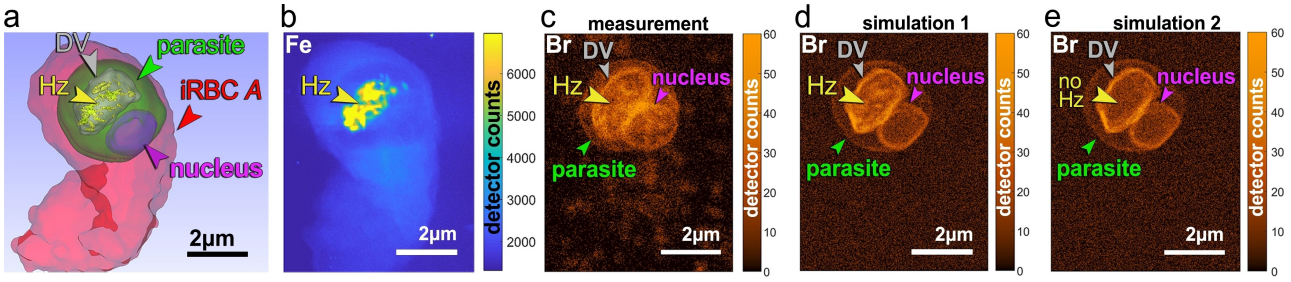

Figure 13. Surface rendering, measured and simulated X-ray fluorescence maps of a bromoquine (BrQ)-treated iRBC. a) Various compartments of the infected cell rendered in color, as derived from a soft X-ray tomography segmentation. b), c) Measured Fe and Br X-ray fluorescence maps of the RBC. d) Simulated Br X-ray fluorescence map. Br atoms were evenly distributed over the surface of the DV membrane, the parasite nucleus, and the parasite membrane with a density of 5×10^3 atoms/µm^2, and on the surface of Hz crystals with a density corresponding to 10% bromoquine surface coverage. e) The same simulation as in (d), but without Br on the surface of the hemozoin crystals.

by Dubar et al.,[63] who reported the presence of the quinoline drug, ferroquine, close to the digestive vacuole membrane of a *Plasmodium*-infected red blood cell imaged by transmission electron microscopy, and by Woodland et al.,[67] who employed visible light fluorescence microscopy to locate covalently labeled chloroquine at the digestive vacuole membrane and other parasitic membranes.

The high concentration of bromoquine at the membrane was explained as being a consequence of complexation of the drug with the remaining free hematin dimers in the lumen of the digestive vacuole, which are hydrophobic and sparsely soluble in the aqueous medium. This property of heme drives the complex towards the digestive vacuole membrane, as shown schematically in the inset to Figure 6. We assume the membrane is eventually perforated leading to spillage of the bromoquine–hematin dimer complex into the interior of the parasite.

8. Conclusions and Perspectives

Crystallization of the malaria pigment hemozoin by the parasite *P. falciparum* is its Achilles' heel and so deserving of a comprehensive review.

We have developed a model of the nucleation and growth of the malaria pigment crystals, based on experimental observations by a wide variety of analytical imaging methods using intact, fully hydrated cells. The heme is sparsely soluble in water, but the lumen of the parasitic digestive vacuole, namely its inside space, is water-filled. So how do the hematin dimers navigate in the aqueous medium and nucleate and grow into uniformly shaped crystals. A model had been reported that the crystals are each formed in a lipid droplet based on an interpretation of electron microscopy images. Such lipid-engulfed crystals have not, however, been detected by soft X-ray tomography, which is uniquely sensitive to carbon density. Rather, hemozoin crystals with their {100} faces in contact with the digestive vacuole membrane in trophozoite stage parasites

were observed, indicating membrane-induced nucleation of hemozoin.

The conundrum of regular hemozoin growth in the aqueous medium, however, remained unresolved. This question was addressed by correlative X-ray microscopy. It proved possible to obtain a measure of the rate of growth of hemozoin crystals. This rate of ~3500 hematin dimers/s was by and large constant during the parasitic trophozoite stage. It was also possible to determine the amount of hemoglobin in the digestive vacuole for a mid-stage trophozoite as sufficient for 30 minutes of protein digestion at the rate of ~1750 molecules/s, which constantly liberates heme that needs to be crystallized at the concomitant rate of ~3500 dimers/s.

According to X-ray and electron imaging of infected red blood cells in the schizont stage, about 50 ± 20 well-shaped hemozoin crystals of average size $130 \times 130 \times 450$ nm^3 had been formed. To achieve this crystalline development, an assembly-line process was assumed: the crystals nucleate and grow, by and large simultaneously, in different parts of the digestive vacuole during the trophozoite stage. Consequently, an average of $3500/(50 \pm 20) \approx 70 \pm 30$ hematin dimers/s are supplied per crystal. Given that the heme detoxification protein (HDP) is identified as an inducer of heme dimerization on release from hemoglobin, we further assume that the different parts of the digestive vacuole lumen each contains a "cluster" of HDPs to synthesize the hematin dimers.

As part of the assembly-line process of hemoglobin degradation, heme release, dimerization and crystallization, we had proposed a feedback mechanism in which coupling exists between the rate of hemoglobin digestion and that of heme dimerization and crystallization. This model is supported by the role played by a lipocalin-like protein, PV5, to control heme crystallization in rodent and human malaria parasites.[42]

The structure of synthetic hemozoin comprises 3 or 4 different isomeric dimers.[44] A subset thereof may act as crystalline self-poisoners on growth, in agreement with the lath habit of synthetic hemozoin. By contrast, the biogenic and theoretical growth form hemozoin crystals have approximate square cross-sections. This difference suggested that the enzymatic process of biogenic heme dimerization is a matter of both speed and the formation of minimum types of dimeric isomers. Hence, a model was envisaged that heme monomers released from oxygenated hemoglobin, yet still coordinated to O_2 at one particular side of the heme ring, would form only one isomeric type on dimerization. The crystal structure of hemozoin was, however, not determined with sufficient accuracy via powder X-ray diffraction to verify the model. A more recent study, which involved low temperature (93 K) electron diffraction measurements on 30 hemozoin crystals, yielded concrete results. The diffraction data has revealed a mixture of one dominant chiral dimer and a minor fraction of the more stable centrosymmetric isomer. This result provides convincing evidence of the role played by the heme detoxification protein as a catalyst of formation of the hematin dimers constituting the malaria pigment. A caveat remains insofar that the blood used in laboratory culture of the parasites was poorly oxygenated. Otherwise, we might have expected hemozoin crystals rich in chiral dimers with a single configuration were the heme detoxification protein and heme coordinated to O_2 to operate in tandem.

Armed with knowledge of the internal and surface structure of hemozoin, it became possible to probe the binding of quinolines and other antimalarials to the faces of hemozoin, and more importantly, how would such a process be toxic to the parasite. Antimalarials, such as quinine and chloroquine, may cap onto various hemozoin faces by acid-base interactions. Drugs such as quinine and mefloquine may, by perhaps forming an O–Fe coordination bond with a heme monomer, also bind to hemozoin as a "tailor-made" inhibitor. Models have been constructed of artemisinin-heme adducts as tailor-made inhibitors, in keeping with artemisinin retardation of hemozoin formation, but which has been demonstrated only in cell-free conditions.

We established the mode of action of a chloroquine-type drug within hydrated malaria parasites in their native, albeit rapidly frozen, environment by correlative X-ray microscopy. Use was made of bromoquine to take advantage of the Br X-ray fluorescence signal. The drug reached sub-millimolar concentration in the digestive vacuole, exceeding that in the culture medium 1000-fold. Moreover, 5–15% of the hemozoin crystal surface was covered with the drug, an amount sufficient to prevent newly liberated heme from docking onto the crystal surfaces. An anticipated consequence of bromoquine smothering the hemozoin surfaces is the high drug concentration found at the digestive vacuole membrane. This was rationalized as a result of drug complexation with free hematin dimers in the digestive vacuole lumen, driving these complexes toward the vacuole membrane. We assume the membrane is eventually perforated leading to spillage of the drug-hematin dimer complex into the interior of the parasite cytoplasm.

Questions are still abound on the topics described here, and need to be addressed. For example, is it possible to clarify whether artemisinin reacts with heme to form tailor-made growth inhibitors of hemozoin. The results described here also suggest that a similar approach should help elucidate how hemozoin is formed in other blood-consuming parasites such as the blood fluke *S. mansoni* and the kissing bug *R. prolixus*.[68] Last, but not least, we hope that this review will be of some use for the design, and understanding of new antimalarial drugs.[69]

Acknowledgements

The authors thank Daniel Goldberg, Michael McBride, Örn Almarsson and James G. McNally for discussions, and Isabella Weissbuch and Gerd Schneider for critical reading of this manuscript. S.K. was supported by the EMBO and the Carlsberg Foundation postdoctoral fellowships. The most recent and unpublished research discussed in this publication was supported by DanScatt, IB Hendriksens Fond and by the project CALIPSOplus under the Grant Agreement 730872 from the EU Framework Programme for Research and Innovation HORIZON 2020. Measurements conducted at synchrotron facilities described in this Review, and spanning over more than a decade, were carried out at the

U41-TXM beamline, Helmholtz-Zentrum Berlin (HZB), at the MISTRAL beamline, ALBA synchrotron light source, at the ID16a beamline, ESRF, at the microXAS beamline at the Swiss Light Source (SLS), at the BW1 beamline, HASYLAB, DESY and at the Electron Bio-Imaging Centre, Diamond Light Source. We thank the beamline teams and HZB, ALBA, ESRF, SLS, DESY for the allocation of synchrotron radiation beamtime and Diamond for electron imaging and diffraction. We thank all the people who supported and were involved in this work over the course of years, as well as organizations for financial support.

Conflict of Interest

The authors declare no conflict of interests.

Keywords: crystal growth · crystal structure · malaria · hemozoin nucleation · mode of action · X-ray imaging

[1] A. C. Uhlemann, S. Krishna, in *Malaria: Drugs, Disease and Post-genomic Biology* (Eds.: R. W. Compans, M. D. Cooper, T. Honjo, H. Koprowski, F. Melchers, M. B. A. Oldstone, S. Olsnes, M. Potter, P. K. Vogt, H. Wagner, D. J. Sullivan, S. Krishna), Springer, Berlin, **2005**, pp. 39–53.
[2] *World Malaria Report 2020: 20 years of global progress and challenges*, World Health Organization, **2020**, https://www.who.int/publications/i/item/9789240015791.
[3] *COVID-19 threatens global progress against malaria, warns UN health agency*, UN News, **2020**, https://news.un.org/en/story/2020/11/1078752.
[4] E. Hempelmann, T. J. Egan, *Trends Parasitol.* **2002**, *18*, 11.
[5] Z. Bozdech, M. Llinás, B. L. Pulliam, E. D. Wong, J. Zhu, J. L. DeRisi, *PLoS Biol.* **2003**, *1*, e5.
[6] H. Meckel von Hemsbach, *Allgemeine Z. Psychiatrie und Psychisch-Gerichtliche Med.* **1847**, *4*, 198–226.
[7] R. Virchow, *Arch. Pathol. Anatomie und Physiol. klinische Medicin* **1849**, *2*, 587–598.
[8] T. Carbone, *G. R. Accad. Med. Torino* **1891**, *39*, 901–906.
[9] A. Laveran, *Paludism, Vol. 146*, New Sydenham Society, **1893**.
[10] R. Ross, *Memoirs: With a Full Account of the Great Malaria Problem and Its Solution*, John Murray, **1923**.
[11] C. D. Fitch, P. Kanjananggulpan, *J. Biol. Chem.* **1987**, *262*, 15552–15555.
[12] A. Slater, W. J. Swiggard, B. R. Orton, W. D. Flitter, D. E. Goldberg, A. Cerami, G. B. Henderson, *Proc. Natl. Acad. Sci. USA* **1991**, *88*, 325–329.
[13] E. Hempelmann, H. M. Marques, *J. Pharmacol. Toxicol. Methods* **1994**, *32*, 25–30.
[14] E. Hempelmann, *Parasitol. Res.* **2007**, *100*, 671–676.
[15] S. Pagola, W. P. Stephens, D. S. Bohle, A. D. Kosar, S. K. Madsen, *Nature* **2000**, *404*, 307–310.
[16] M. F. Oliveira, S. W. Kycia, A. Gomez, A. J. Kosar, D. S. Bohle, E. Hempelmann, D. Menezes, M. A. Vannier-Santos, P. L. Oliveira, S. T. Ferreira, *FEBS Lett.* **2005**, *579*, 6010–6016.
[17] N. Klonis, R. Dilanian, E. Hanssen, C. Darmanin, V. Streltsov, S. Deed, H. Quiney, L. Tilley, *Biochemistry* **2010**, *49*, 6804–6811.
[18] a) D. Jani, R. Nagarkatti, W. Beatty, R. Angel, C. Slebodnick, J. Andersen, S. Kumar, D. Rathore, *PLoS Pathog.* **2008**, *4*, e1000053; b) K. Nakatani, H. Ishikawa, S. Aono, Y. Mizutani, *Sci. Rep.* **2014**, *4*, 6137 (6131-6137).
[19] a) D. J. Sullivan, I. Y. Gluzman, D. G. Russell, D. E. Goldberg, *Proc. Natl. Acad. Sci. USA* **1996**, *93*, 11865–11870; b) D. J. Sullivan, H. Matile, R. G. Ridley, D. E. Goldberg, *J. Biological Chemistry* **1998**, *273*, 31103–31107.
[20] I. Weissbuch, L. Leiserowitz, *Chem. Rev.* **2008**, *108*, 4899–4914.
[21] R. Buller, M. L. Peterson, Ö. Almarsson, L. Leiserowitz, *Cryst. Growth Des.* **2002**, *2*, 553–562.
[22] G. S. Noland, N. Briones, D. J. Sullivan, *J. Mol. Biochem. Parasitol.* **2003**, *130*, 91–99.
[23] I. Solomonov, M. Osipova, Y. Feldman, C. Baehtz, K. Kjaer, I. K. Robinson, G. T. Webster, D. McNaughton, B. R. Wood, I. Weissbuch, L. Leiserowitz, *J. Am. Chem. Soc.* **2007**, *129*, 2615–2627.
[24] D. J. Sullivan, I. Y. Gluzman, D. E. Goldberg, *Science* **1996**, *271*, 219–222.
[25] a) J. M. Pisciotta, I. Coppens, A. K. Tripathi, P. F. Scholl, J. Schuman, S. Bajad, V. Shulaev, D. J. Sullivan, *Biochem. J.* **2007**, *402*, 197–204; b) T. J. Egan, *J. Inorg. Biochem.* **2008**, *102*, 1288–1299; c) K. N. Olafson, M. A. Ketchum, J. D. Rimer, P. G. Vekilov, *Proc. Natl. Acad. Sci. USA* **2015**, *112*, 4946–4951; d) P. G. Vekilov, J. D. Rimer, K. N. Olafson, M. A. Ketchum, *CrystEngComm* **2015**, *17*, 7790–7800.
[26] C. D. Fitch, G. Z. Cai, Y. F. Shen, D. J. Shoemaker, *Biochim. Biophys. Acta* **1999**, *1454*, 31–37.
[27] A. Sorrentino, J. Nicolas, R. Valcarcel, F. J. Chichon, M. Rosanes, J. Avila, A. Tkachuk, J. Irwin, S. Ferrer, E. Pereiro, *J. Synchrotron Radiat.* **2015**, *22*, 1112–1117.
[28] G. Schneider, *Ultramicroscopy* **1998**, *75*, 85–104.
[29] T. J. Egan, J. Y. Chen, K. A. de Villiers, T. E. Mabotha, K. J. Naidoo, K. K. Ncokazi, S. J. Langford, D. McNaughton, S. Pandiancherri, B. R. Wood, *FEBS Lett.* **2006**, *580*, 5105–5110.
[30] K. A. de Villiers, M. Osipova, T. E. Mabotha, I. Solomonov, Y. Feldman, K. Kjaer, I. Weissbuch, T. J. Egan, L. Leiserowitz, *Cryst. Growth Des.* **2009**, *9*, 626–632.
[31] A. N. Hoang, K. K. Ncokazi, K. A. de Villiers, D. W. Wright, T. J. Egan, *Dalton Trans.* **2010**, *39*, 1235–1244.
[32] a) I. Weissbuch, M. Lahav, L. Leiserowitz, *Cryst. Growth Des.* **2003**, *3*, 125–150; b) I. Kuzmenko, H. Rapaport, K. Kjaer, J. Als-Nielsen, I. Weissbuch, M. Lahav, L. Leiserowitz, *Chem. Rev.* **2001**, *101*, 1659–1696.
[33] X. Wang, E. Ingall, B. Lai, A. G. Stack, *Cryst. Growth Des.* **2010**, *10*, 798–805.
[34] D. Goldberg, A. F. G. Slater, A. Cerami, G. B. Henderson, *Proc. Natl. Acad. Sci. USA* **1990**, *87*, 2931–2935.
[35] S. Kapishnikov, T. Berthing, L. Hviid, M. Dierolf, A. Menzel, F. Pfeiffer, J. Als-Nielsen, L. Leiserowitz, *Proc. Natl. Acad. Sci. USA* **2012**, *109*, 11184–11187.
[36] a) E. Hanssen, C. Knoechel, M. Dearnley, M. W. A. Dixon, M. L. Gros, C. Larabell, L. Tilley, *J. Struct. Biol.* **2011**, *177*, 224–232; b) E. Hanssen, C. Knoechel, N. Klonis, N. Abu-Bakar, S. Deed, M. LeGros, C. Larabell, L. Tilley, *J. Struct. Biol.* **2011**, *173*, 161–168.
[37] a) S. Kapishnikov, A. Weiner, E. Shimoni, G. Schneider, M. Elbaum, L. Leiserowitz, *Langmuir* **2013**, *29*, 14595–14602; b) S. Kapishnikov, A. Weiner, E. Shimoni, P. Guttmann, G. Schneider, N. Dahan-Pasternak, R. Dzikowski, L. Leiserowitz, M. Elbaum, *Proc. Natl. Acad. Sci. USA* **2012**, *109*, 11188–11193.
[38] S. Kapishnikov, D. Grolimund, G. Schneider, E. Pereiro, J. G. McNally, J. Als-Nielsen, L. Leiserowitz, *Sci. Rep.* **2017**, *7*, 7610.
[39] M. Chugh, V. Sundararaman, S. Kumar, V. S. Reddy, W. A. Siddiqui, K. D. Stuart, P. Malhotra, *Proc. Natl. Acad. Sci. USA* **2013**, *110*, 5392–5397.
[40] K. Nakatani, H. Ishikawa, S. Aono, Y. Mizutani, *Biochem. Biophys. Res. Commun.* **2013**, *439*, 477–480.
[41] S. Kapishnikov, L. Leiserowitz, Y. Yang, P. Cloetens, E. Pereiro, F. Awamu Ndonglack, K. Matuschewski, J. Als-Nielsen, *Sci. Rep.* **2017**, *7*, 802.
[42] J. M. Matz, B. Drepper, T. B. Blum, E. van Genderen, A. Burrell, P. Martin, T. Stach, L. M. Collinson, J. P. Abrahams, K. Matuschewski, M. J. Blackman, *Proc. Natl. Acad. Sci. USA* **2020**, *117*, 16546.
[43] L. Leiserowitz, F. Nader, *Acta Crystallogr. Sect. B* **1977**, *33*, 2719–2733.
[44] a) T. Straasø, N. Marom, I. Solomonov, L. K. Barfod, M. Burghammer, R. Feidenhans'l, J. Als-Nielsen, L. Leiserowitz, *Cryst. Growth Des.* **2014**, *14*, 1543–1554; b) T. Straasø, S. Kapishnikov, K. Kato, M. Takata, J. Als-Nielsen, L. Leiserowitz, *Cryst. Growth Des.* **2011**, *11*, 3342–3350.
[45] D. S. Bohle, E. L. Dodd, P. W. Stephens, *Chem. Biodiversity* **2012**, *9*, 1891–1902.
[46] N. Marom, A. Tkatchenko, S. Kapishnikov, L. Kronik, L. Leiserowitz, *Cryst. Growth Des.* **2011**, *11*, 3332–3341.
[47] a) I. Weissbuch, R. Popovitz-Biro, M. Lahav, L. Leiserowitz, *Acta Crystallogr. Sect. B* **1995**, *51*, 115–148; b) I. Weissbuch, L. Addadi, L. Leiserowitz, *Science* **1991**, *253*, 637–645.
[48] R. A. Dilanian, V. Streltsov, H. D. Coughlan, H. M. Quiney, A. V. Martin, N. Klonis, C. Dogovski, S. Boutet, M. Messerschmidt, G. J. Williams, *J. Appl. Crystallogr.* **2017**, *50*, 1533–1540.
[49] M. Nitzan, H. Taitelbaum, *IEEE Instrumentation & Measurement Magazine* **2008**, *11*, 9–15.
[50] D. Waterman, D. Mullick, T. Gruene, P. Zhang, L. Leiserowitz, M. Elbaum, et al. **2021**, unpublished results.
[51] C. M. Poser, G. W. Bruyn, *An Illustrated History of Malaria*, Parthenon Publishing Group, **1999**.
[52] a) M. Delépine, *J. Chem. Educ.* **1951**, *28*, 454–461; b) P. J. Pelletier, J.-B. Caventou, *Recherches Chimiques sur les Quinquinas, Vol. 15*, Crochard, **1820**.

[53] a) C. D. Fitch, *Science* **1970**, *169*, 289–290; b) F. Verdier, J. Le Bras, F. Clavier, I. Hatin, M. Blayo, *Antimicrob. Agents Chemother.* **1985**, *27*, 561–564.
[54] P. G. Bray, S. A. Ward, P. M. O'Neill in *Current Topics in Microbiology and Immunology, Vol. 295: Drugs, Disease and Post-genomic Biology* (Eds.: D. J. Sullivan, S. Krishna), Springer, Berlin, **2005**, pp. 3–38.
[55] K. A. de Villiers, H. M. Marques, T. J. Egan, *J. Inorg. Biochem.* **2008**, *102*, 1660–1667.
[56] A. Robert, Y. Coppel, B. Meunier, *Chem. Commun.* **2002**, 414–415.
[57] F. Dubar, T. J. Egan, B. Pradines, D. Kuter, K. K. Ncokazi, D. Forge, J.-F. Paul, C. Pierrot, H. Kalamou, J. Khalife, E. Buisine, C. Rogier, H. Vezin, I. Forfar, C. Slomianny, X. Trivelli, S. Kapishnikov, L. Leiserowitz, D. Dive, C. Biot, *ACS Chem. Biol.* **2011**, *6*, 275–287.
[58] G. R. Desiraju, T. Steiner, *Structural Chemistry and Biology, Vol. 9: The Weak Hydrogen Bond*, International Union of Crystal, **1999**.
[59] Y. L. Hong, Y. Z. Yang, S. R. Meshnick, *Mol. Biochem. Parasitol.* **1994**, *63*, 121–128.
[60] a) A. Robert, J. Cazelles, B. Meunier, *Angew. Chem. Int. Ed.* **2001**, *40*, 1954–1957; *Angew. Chem. Int. Ed.* **2001**, *113*, 2008–2011; b) A. Robert, B. Meunier, *J. Am. Chem. Soc.* **1997**, *119*, 5968–5969; c) A. Robert, F. Benoit-Vical, C. Claparols, B. Meunier, *Proc. Natl. Acad. Sci. USA* **2005**, *102*, 13676.
[61] A. V. Pandey, B. L. Tekwani, R. L. Singh, V. S. Chauhan, *J. Biol. Chem.* **1999**, *274*, 19383–19388.
[62] a) K. N. Olafson, T. Q. Nguyen, J. D. Rimer, P. G. Vekilov, *Proc. Natl. Acad. Sci. USA* **2017**, *114*, 7531–7536; b) J. Gildenhuys, T. l Roex, T. J. Egan, K. A. de Villiers, *J. Am. Chem. Soc.* **2013**, *135*, 1037–1047.
[63] F. Dubar, S. Bohic, C. Slomianny, J.-C. Morin, P. Thomas, H. Kalamou, Y. Guérardel, P. Cloetens, J. Khalife, C. Biot, *Chem. Commun.* **2012**, *48*, 910–912.
[64] a) S. R. Vippagunta, A. Dorn, H. Matile, A. K. Bhattacharjee, J. M. Karle, W. Y. Ellis, R. G. Ridley, J. L. Vennerstrom, *J. Med. Chem.* **1999**, *42*, 4630–4639; b) D. De, F. M. Krogstad, L. D. Byers, D. J. Krogstad, *J. Med. Chem.* **1998**, *41*, 4918–4926.
[65] S. R. Hawley, P. G. Bray, M. Mungthin, J. D. Atkinson, P. M. O'Neill, S. A. Ward, *Antimicrob. Agents Chemother.* **1998**, *42*, 682–686.
[66] S. Kapishnikov, T. Staalsø, Y. Yang, J. Lee, A. J. Pérez-Berná, E. Pereiro, Y. Yang, S. Werner, P. Guttmann, L. Leiserowitz, J. Als-Nielsen, *Proc. Natl. Acad. Sci. USA* **2019**, *116*, 22946–22952.
[67] J. G. Woodland, R. Hunter, P. J. Smith, T. J. Egan, *ACS Chem. Biol.* **2018**, *13*, 2939–2948.
[68] a) J. R. Silva, F. B. Mury, M. F. Oliveira, P. L. Oliveira, C. P. Silva, M. Dansa-Petretski, *Insect Biochem. Mol. Biol.* **2007**, *37*, 523–531; b) J. B. R. Corrêa Soares, C. M. Maya-Monteiro, P. R. B. Bittencourt-Cunha, G. C. Atella, F. A. Lara, J. C. P. d'Avila, D. Menezes, M. A. Vannier-Santos, P. L. Oliveira, T. J. Egan, M. F. Oliveira, *FEBS Lett.* **2007**, *581*, 1742–1750.
[69] J. Wiesner, R. Ortmann, H. Jomaa, M. Schlitzer, *Angew. Chem. Int. Ed.* **2003**, *42*, 5274–5293; *Angew. Chem.* **2003**, *115*, 5432–5451.

Manuscript received: November 17, 2020
Accepted manuscript online: February 1, 2021
Version of record online: March 19, 2021